Structure/function of the soluble guanylyl cyclase catalytic domain

Kenneth C. Childers, **Elsa D. Garcin**[*]

University of Maryland Baltimore County, Department of Chemistry and Biochemistry, Baltimore, USA

Abstract

Soluble guanylyl cyclase (GC-1) is the primary receptor of nitric oxide (NO) in smooth muscle cells and maintains vascular function by inducing vasorelaxation in nearby blood vessels. GC-1 converts guanosine $5'$-triphosphate (GTP) into cyclic guanosine $3',5'$-monophosphate (cGMP), which acts as a second messenger to improve blood flow. While much work has been done to characterize this pathway, we lack a mechanistic understanding of how NO binding to the heme domain leads to a large increase in activity at the C-terminal catalytic domain. Recent structural evidence and activity measurements from multiple groups have revealed a low-activity cyclase domain that requires additional GC-1 domains to promote a catalytically-competent conformation. How the catalytic domain structurally transitions into the active conformation requires further characterization. This review focuses on structure/function studies of the GC-1 catalytic domain and recent advances various groups have made in understanding how catalytic activity is regulated including small molecules interactions, Cys-S-NO modifications and potential interactions with the NO-sensor domain and other proteins.

Keywords

Soluble guanylyl cyclase; Adenylyl cyclase; Catalytic domain; Nitric oxide; S-nitrosation; Activation mechanism

1. Introduction

Soluble guanylyl cyclase (GC-1) maintains vascular function through the NO/GC-1/cGMP pathway [1,2] by catalyzing the conversion of GTP into cGMP (Fig. 1). The GC-1 heme prosthetic group binds NO with pi-comolar affinity, resulting in a 100- to 200-fold increase in catalytic activity. cGMP activates protein kinase G, which phosphorylates a myriad of targets to induce, among other effects, vasodilation and inhibition of platelet aggregation and adhesion to the arterial wall. Dysfunction in the NO/GC-1/cGMP pathway through reactive oxygen species (ROS) has been linked to a variety of vascular diseases [3,4]. ROS

[*]Corresponding author. University of Maryland Baltimore County, Department of Chemistry and Biochemistry, 1000 Hilltop Circle, Baltimore, MD 21250, USA. egarcin@umbc.edu (E.D. Garcin).

can disrupt this pathway by reacting with free NO, thus reducing NO bioavailability, or oxidizing the ferrous heme group in GC-1, causing it to lose its sensitivity toward NO. GC-1 has a significantly lower affinity for oxidized heme [5]. Once the heme is lost, apo-GC-1 is targeted for degradation [6].

Cardiovascular diseases are responsible for the highest mortality rate globally with approximately 1 in 3 deaths being attributed to a cardio-related illness. The role of GC-1 in maintaining vascular health makes it an ideal target to improve cardiovascular function. Pharmaceuticals that elevate GC-1 activity are classified as either heme-dependent (stimulators) or heme-independent (activators; reviewed in Ref. [7]). In 2013, riociguat became the first FDA-approved stimulator to target GC-1 for the treatment of pulmonary arterial hypertension and chronic thromboembolic pulmonary hypertension (CTEPH). Clinical trials in CTEPH patients showed treatment with riociguat improved 6-min walking distances and reduced pulmonary blood pressure over the placebo group [8]. Cinaciguat and ataciguat are known GC-1 activators. Structural evidence using a bacterial homolog of the NO-sensor domain with bound cinaciguat suggested the activator rescues GC-1 activity under oxidative stress by occupying the empty heme pocket and making key interactions with nearby residues while mimicking the NO-severed His ligand [9]. This hypothesis was supported by studies showing that cinaciguat improved cGMP production in endothelial cells after oxidative damage [6]. Further clinical trials with cinaciguat found hypotensive side-effects when treating patients for acute heart failure [10] and were ceased by the FDA in 2011. Treatment of rat aortic smooth muscle cells with ataciguat under oxidative stress improved basal and NO-stimulated GC-1 activity [11]. Ongoing clinical trials are using ataciguat as a treatment for aortic stenosis due to calcification. More recently, studies using the biotinylated IWP-854 GC-1 stimulator helped to identify a conserved binding site for other GC-1 stimulators in the βHNOX NO-sensor domain [12]. Elucidating this binding region could provide the foundation for a class of novel GC-1 stimulators.

A dysfunctional NO/GC-1/cGMP pathway has been implicated in other vasculature disorders. Glaucoma is a leading cause of blindness in the United States with approximately 2 million people afflicted and is characterized by increased intraocular pressure (IOP) and damage to the optic nerve. Primary open-angle glaucoma (POAG) is a subtype of glaucoma and has no known underlying etiology. Treatment for POAG manages symptoms through beta-blockers to reduce aqueous humor inflow and eye surgery to relieve IOP [13]. Multiple groups have identified a dysfunctional NO/GC-1/cGMP pathway as an alternate target for POAG treatment (reviewed in Ref. [4]). NO-donors and cGMP have been used in POAG animal studies to lower IOP [14,15]. Older mice lacking the αGC-1 polypeptide had typical POAG symptoms including reduced aqueous humor outflow, increased IOP, and damage to the optic nerve [16], directly implicating GC-1 in the disease. More recently, treatment of mouse eyes with elevated IOP and reduced aqueous humor outflow using a novel GC-1 stimulator improved ocular flow rate over the vehicle-treated group; similar results were observed using an NO-donor [17]. Targeting the NO/GC-1/cGMP pathway for improved optic blood flow may prove useful in the treatment of POAG.

Renal disease is characterized by aberrant fibrotic remodeling of renal tissue, elevated apoptosis in kidney tissue, and eventual organ failure. In addition, patients with renal disease

are more likely to suffer from systemic hypertension due to oxidative damage (reviewed in Ref. [18]). Treatment of rats with progressive renal fibrosis using GC-1 stimulator BAY 41-2272 elevated cGMP levels and reduced kidney fibrosis and systemic blood pressure [19]. Rat models of renal disease induced by a high-salt diet were given cinaciguat. After 21 weeks, increased cGMP levels were measured and renal function was improved over the placebo group [20]. NO supplementation has also been used to improve renal function. After 1 week of supplemented dietary arginine, the substrate for NO synthesis, increased cGMP levels were measured in urine, improved renal function and reduced renal fibrosis and apoptosis [21].

Because of the systemic role GC-1 has in vasculature-related illnesses and the fact that there is only one FDA-approved drug that targets GC-1, a complete understanding of how NO stimulates GC-1 activity is crucial. In this review, we provide a comprehensive overview of the GC-1 catalytic domain. We also discuss recent implications for Cys-S-NO modifications in the catalytic domain regulating GC-1 activity and interactions with the NO-sensor domain.

2. GC-1 domain architecture

GC-1 is a 150 kDa heterodimer and its $\alpha_1\beta_1$ isoform is found ubiquitously. While another isoform of the enzyme does exist (GC-2; $\alpha_2\beta_1$) [22], this review will focus on the predominant $\alpha_1\beta_1$ isoform. Each α/β polypeptide contains four domains from N- to C-terminus connected by short linkers: NO-sensor domain, PAS domain, coiled-coil domain, and catalytic domain (Fig. 2). The N-terminal NO-sensor domain is predicted to adopt a structure similar to bacterial heme nitric oxide-oxygen binding (HNOX) proteins (Fig. 2). These proteins are typically standalone proteins and use a heme cofactor to sense gaseous ligands and activate response proteins to elicit the desired effect, usually through gene regulation [23]. While αHNOX and βHNOX domains are predicted to share a similar HNOX-like fold, only the βHNOX domain of GC-1 carries a heme prosthetic group that binds NO; the role of αHNOX remains to be determined, however recent work suggests it regulates GC-1 activity by lowering the affinity of βHNOX for CO and NO [24]. βHNOX uses a His ligand to bind the heme cofactor in its reduced Fe^{2+} redox state. NO binding to the distal heme side severs the His-iron bond, which is thought to play a crucial role in NO-induced stimulation of GC-1 [25,26]. In addition, several groups have found that excess NO is required to fully activate GC-1 [27,28]. The proximal side of the heme [28,29] or Cys residues [30,31] have been suggested as potential binding sites for the extra NO. However, recent spectroscopic data in *Shewanella oneidensis* HNOX shows that the distal site is preferred, thus questioning the biological significance of proximal heme-NO binding [32].

The subsequent domain belongs to the Per-Arnt-Sim (PAS) family of proteins, typically used to transduce signals to effector domains through subtle conformational shifts. While some PAS domains use cofactors for signal transduction, the PAS domain in GC-1 has none. Crystal structures of a bacterial homolog [33] and of the GC-1 αPAS domain [34] have been solved and show the predicted fold consisting of six β-sheets surrounded by several short α helices (Fig. 2). The GC-1 PAS domain has been suggested to play a key role in GC-1

dimerization [33]. More recently, the PAS domain was shown to interact with heat-shock protein 90 and mediate heme insertion in the βHNOX domain [35].

Crystallographic studies showed that the coiled-coil (CC) domain folds as long α-helices (Fig. 2) in an antiparallel orientation [36]. However cross-linking studies later demonstrated that the heterodimeric CC assembles in a parallel orientation [37]. The CC domain has been shown to play a key role in GC-1 heterodimerization [38], and to act as a scaffold for other GC-1 domains [37,39].

The C-terminal catalytic domain (αβGC^{cat}) contains the substrate-binding pocket located at the interface of the α and β subunits, which both contribute key residues for GTP binding (Fig. 2). Several structures of apo inactive cyclase domains from bacteria, algae, fungus, and human have been solved, but a structure of the holo active form remains elusive [40–44]. Several groups have reported a high propensity for ββGC^{cat} homodimers to form both in solution and during crystallization attempts [42,43]. Despite these structural characterizations, several key questions remain about the αβGC^{cat} domain: what is the mechanism by which αβGC^{cat} transitions from the inactive apo conformation to the catalytically-active conformation upon NO binding? What are the residues involved in the transition from inactive to active αβGC^{cat}? How is the NO-activating signal transduced from the N-terminal NO-sensor domain to the C-terminal catalytic domain? Answering these questions will aid in the design of novel therapeutics that target GC-1 and promote NO-sensitization and cGMP generation.

3. Structural studies of the cyclase catalytic domains

3.1. The homologous adenylyl cyclase enzyme

Much of what we know about the αβGC^{cat} domain structure comes from studies of the homologous adenylyl cyclase (AC) catalytic domain. AC converts ATP into cAMP and is composed of two membrane-bound helical domains and two cytosolic catalytic domains, termed C1 and C2. Sequence alignment identifies C1 as the αGC^{cat} counterpart and C2 as the βGC^{cat} counterpart with ~30% sequence identity for both alignments. Much like the αβGC^{cat} domain, C1 and C2 must come together to form the ATP-binding cleft. AC maintains a low cAMP turnover rate, but two known stimulators increase its activity. $G_{s\alpha}$, a subunit of the G-protein coupled receptor, increases AC activity 5-fold and forskolin, a small diterpene molecule isolated from the plant *C. forskohlii*, increases AC activity 9-fold [45]. The x-ray structure of an inactive C2/C2 homodimer was solved (Fig. 3a) and showed forskolin bound to each monomer in a well-characterized hydrophobic pocket at the dimer interface [46]. Based on these results, it was hypothesized that forskolin activates AC via favorable burying of hydrophobic regions to stabilize the C1/C2 heterodimer. The structure of the C1/ C2 heterodimer was solved in the closed conformation (Fig. 3b) with bound activators $G_{s\alpha}$ and forskolin, and a non-cyclizable ATP substrate [47]. This structure confirmed the identity of the residues important for catalysis and nucleobase specificity (Table 1). Binding of $G_{s\alpha}$ via insertion of its switch II helix into a groove of the C2 subunit is thought to reorient catalytic residues in the C1/C2 heterodimer into a competent conformation and bury additional exposed hydrophobic regions near the membrane. C1/C2 conformational changes also include a 7° rigid-body rotation of C1 around C2 and closure

of the ATP-binding pocket. While there is no known allosteric activator for GC-1 that binds in the $\alpha\beta GC^{cat}$ domain, similar conformational transitions are predicted for its catalytic domain (see sections 3.3–3.5).

There exist nine isoforms of the membrane-bound AC and each have discrete physiological functions [48]. Because each isoform utilizes a conserved C1/C2 catalytic domain to cyclize ATP [49], there is a need for isoform-specific activators and inhibitors. Derivatives of forskolin have been screened using computational docking to find stimulators of isoform AC-VI [50], which is thought to play a beneficial role in cardiac function. These forskolin-analogs are predicted to bind in the forskolin-binding pocket and make extended interactions outside of the conserved binding site for isoform-specificity [51]. Others have shown that adenine-based small molecules can promiscuously bind to and inhibit multiple AC isoforms [52]. Inhibitors utilizing a hydrophobic moiety bound to the $2',3'$-positions of the NTP ribose have recently been shown to bind with nanomolar affinity at the substrate-binding groove, albeit non-isoform specifically (see section 4.4).

3.2. Bacterial guanylyl cyclase

Rauch et al. solved the first structure of a prokaryotic guanylyl cyclase domain from the cyanobacterium *Synechocystis PCC 6803* [40]. This protein contains an N-terminal extracellular sensory CHASE2 domain linked to a C-terminal cyclase Cya2 catalytic domain (GC_{cya2}) via transmembrane segments [53]. The cyclase domain shares 27.7% and 23.9% sequence identity with human βGC^{cat} and αGC^{cat}, respectively (Fig. 4). The protein homodimerizes and contains a Glu-Gly residue pair for nucleobase specificity that sets its apart from its mammalian guanylyl cyclase (Glu-Cys/Ser pair) and adenylyl cyclase (Lys-Asp/Thr pair) counterparts (Table 1). The authors showed that Cya2 has a strong preference and specificity for GTP over ATP, allowing for its classification as the first bacterial guanylyl cyclase. Homodimer formation of Cya2 is strongly dependent on ionic strength, with a K_D of 8 μM for dimer formation. The structure of the Cya2 homodimer confirms a conserved overall fold with class III adenylyl cyclase, despite limited sequence identity (Fig. 3c). Residues from both subunits contribute to formation of the active site(s) at the dimer interface. While two active sites are present in the symmetrical dimer, mutagenesis and activity assays show that a single active site is sufficient. In addition, these studies suggest that the unusual Glu-Gly pair exquisitely modulates the increased GTP specificity of Cya2 over ATP. While the Glu residue plays a major role in selectivity of the base via hydrogen bonding assisted by a supporting Lys residue, the role of the Gly residue may be to provide steric selectivity in concert with a Tyr residue, instead of a role in hydrogen bonding as is observed in AC and possibly other GCs.

Finally, a sequence alignment with other bacterial cyclases suggests that Cya2 may be representative of a bacterial guanylyl cyclase subgroup, raising the interesting question about the exact role played by cGMP in these organisms.

3.3. Eukaryotic guanylyl cyclase

Winger et al. solved the crystal structure of the catalytic domain of the soluble guanylyl cyclase (CYG12) from the eukaryotic green algae *Chlamydomonas reinhardtii* [41]. CYG12

functions as a homodimer and the guanylyl cyclase domain (termed GC_{Cr}) adopts a Chinese yin-yang fold similar to C1/C2 in AC, as expected (Fig. 3d). The homodimer contains two symmetric active sites at the dimer interface. Contrary to the Cya2 guanylyl cyclase [40], CYG12-GC_{Cr} showed positive cooperativity, implying communication between the two sites.

Based on sequence alignments (Fig. 4), superposition with the structure of AC catalytic domain as well as structure modeling [54], the residues involved in GTP binding and catalysis were inferred. While the GC_{Cr} structure was solved in the absence of metal or substrate, key conserved residues include Asp residues binding the metal ions, Asn binding the ribose moiety of GTP, Lys and Arg stabilizing the phosphate moieties, and a canonical Glu-Cys pair for nucleobase specificity (Table 1). Most of these residues were found in locations close to their AC counterparts, highlighting the likely conservation of catalytic mechanisms in both enzymes. Dimethyl-arsenic modification of Cys residues promoted local distortions in structural elements forming the active site, and was cited as a possible cause for failing to observe metal and substrate in the crystal structure. Comparison of this inactive open structure with that of the closed AC structure with metals and substrate analogs (PDB code 1CJU) suggested a possible activation mechanism for CYG12. Tesmer et al. proposed that movements of helices α1 and α4 were key hallmarks of activation in adenylyl cyclases [47]. In the GC_{Cr} structure, both helices adopt conformations also observed in the AC inactive structure, reinforcing the idea that the structure corresponds to the inactive state. Finally, the authors speculated that a groove found at the surface of the monomer B (equivalent to C2 subunit in AC) could provide a docking site for regulators like the HNOX domain, similarly to the $G_s\alpha$ binding pocket in AC. GC_{Cr} shares 44.2% and 40.3% sequence identity with human βGC^{cat} and αGC^{cat} subunits, respectively (Fig. 4). Thus, this structure represented the best model for the human catalytic domain at the time.

3.4. Human mutant guanylyl cyclase

It took almost 5 years for the first structure of human $\alpha\beta GC^{cat}$ to become available [42] and confirm most predictions based on homologous structures and sequence alignments. While crystallizing the $\beta\beta GC^{cat}$ homodimer was straightforward (Fig. 3e), obtaining the heterodimer structure required engineering of an interfacial disulfide bridge, while mutating out one of the natural Cys in βGC^{cat} to avoid favoring $\beta\beta GC^{cat}$ homodimers. Unfortunately, this mutation is inactivating [55,56], and catalytic activity could not be detected for the mutant heterodimer in the presence of Mg^{2+} (Table 2). The human catalytic domains adopt the head-to-tail wreath fold observed in other class III cyclases. The active site is located at the dimer interface and each subunit contributes key residues. While the structure is in the inactive open state, comparison with the C1/C2 AC heterodimer bound to substrate analog ddATP and Mg^{2+} confirms residues important for catalysis: αAsp530 and αAsp486 for Mg^{2+} coordination, αArg574, βArg552, and βLys593 for phosphate tail stabilization, βAsn548 for ribose binding, and the pair βGlu473-βCys541 for nucleobase specificity (Table 1). The Glu-Cys pair has been heralded as the hallmark for GTP specificity. However, GC-1 has been shown to be quite promiscuous compared to other cyclases, and can also generate cAMP, cIMP, and cXMP [57]. A superimposition of the open apo $\alpha\beta GC^{cat}$ structure on the closed ligand-bound C1/C2 AC structure (PDB code 1CJU) suggested

that a much larger conformational change (26° rotation) of the αGC^{cat} subunit would be necessary for activation, as suggested earlier [41]. Finally, a pseudo-symmetric active site is created, but its size is much smaller than in AC, and it remains to be seen whether it can accommodate small molecule activators (Fig. 5).

3.5. Human wild-type guanylyl cyclase

Our lab was the first to solve the structure of the human wild-type $\alpha\beta GC^{cat}$ domain (Fig. 3g and h) in its apo inactive state [43]. Comparison with the mutant heterodimer structure [42] reveals how subtle conformational changes at the dimer interface can affect catalytic activity. In agreement with biochemical and biophysical data, we identified three main regions with the highest degree of sequence conservation: (i) the substrate channel; (ii) the C-terminal subdomain of the αGC^{cat} subunit, which could serve as a docking site to the regulatory HNOX domain, and in agreement with HDXMS studies [58]; and (iii) the dorsal face of the heterodimer containing both N-termini that could serve as the docking site for the coiled-coil domain, again in agreement with HDXMS studies [58]. We identified two structural motifs that likely modulate the orientation of the two subunits with each other and catalytic activity (Fig. 3g and h). The first one is a conserved β-hairpin in the βGC^{cat} subunit (flap-wrap) that wraps onto the αGC^{cat} subunit. In particular, the βMet537Asn mutation in this flap was shown to increase constitutive GC-1 activity and enhance the response to NO/YC-1 [59]. A similar mutation in AC increased both activity and affinity of the C1 and C2 subunits without activators [60]. We proposed that the mutation would promote interactions between the two subunits that may help promote realignment of the catalytic residues for optimal activity. The second structural motif is an interfacial hydrogen-bond network between αGlu526, αCys595, and βThr474, similarly to what was observed in AC. Mutations in this triad that abrogate hydrogen bonds lead to severely impaired catalytic activity in GC-1 [59,61] and AC [60,62], while a conservative mutation (αCys595Ser) lead to increased basal activity in GC-1 [56].

We were the first to show unambiguously that co-purified αGC^{cat} and βGC^{cat} subunits assemble in solution as a complex mixture of monomers, homodimers, and heterodimers [43]. Using size exclusion coupled to multi-angle x-ray scattering, nano-ESI/MS and nano-ESI/ MS/MS, we were able to quantitatively determine for the first time dimerization K_D for ββGCcat homodimers (< 2 μM), αβGCcat heterodimers (~6.9 μM), and $\alpha\alpha GC^{cat}$ homodimers (30 μM). These results are in contrast with previous studies that suggested that the K_D of homodimers was much higher than that of heterodimers [63], most likely because of the difference in the methods used in each study. In addition, salt concentrations may play a role in the rate of dimerization, as discussed in section 3.2. Because mass spectrometry is sensitive to salt, our experiments were performed using non-physiological volatile salt buffers. Regardless, our results are in agreement with our analyses of the dimer interfaces that show that the buried area and number of hydrogen bonds, salt bridges, and hydrophobic interactions are greater in the $\beta\beta GC^{cat}$ homodimers compared to the $\alpha\beta GC^{cat}$ heterodimers. Finally, our results had important implications: when measuring activity of the catalytic domains, choosing a concentration that enables heterodimer formation is critical (i.e. > 10 μM). While doing so will not reduce the amount of $\beta\beta GC^{cat}$ homodimers, higher protein concentrations will increase the amount of $\alpha\beta GC^{cat}$ heterodimers.

Taking this into account, our activity measurements adjusted to the amount of heterodimer revealed that the $\alpha\beta GC^{cat}$ only possess ~0.01% of basal full-length GC-1 activity using Mg^{2+}. The activity of $\alpha\beta GC^{cat}$ increased 779-fold when using Mn^{2+} as a cofactor while full-length GC-1 activity increased by ~2-fold, but $\alpha\beta GC^{cat}$ still showed less than 6% of GC-1 activity (Table 2). Few studies directly compare specific activity of full-length GC-1 and truncated constructs. The published values of specific activity for full-length GC-1 and truncated constructs show great variation (Table 2), even after adjusting for heterodimer amounts and calculating specific activity in fmol/min/pmol of protein (instead of pmol/min/mg of protein). Possible reasons for discrepancy include protein concentrations, temperature, sample purity, heme content of the full-length constructs, and amount of heterodimers for the catalytic constructs. Our results showed that the isolated $\alpha\beta GC^{cat}$ domains are not catalytically competent despite their ability to dimerize. We thus proposed that other GC-1 domains (including the coiled-coil domain) modulate the relative orientation of the catalytic domains and are necessary to promote an optimal conformation of the catalytic domains via structural changes.

3.6. The guanylyl cyclase of the fusion protein RhoGC

Very recently, the structure of the catalytic guanylyl cyclase domain of the fusion protein RhoGC from the aquatic fungus *Blastocladiella emersonii* was solved [44]. The homodimeric transmembrane protein senses light through a rhodopsin domain (residues 176-388) and transduces the signal via a coiled-coil domain to the cytosolic catalytic GC_{Rho} domain (residues 443-626) where GTP can be cyclized for phototaxis [64,65]. Kumar et al. expressed and purified two constructs containing the catalytic domain: GC_{Rho} and $GCwCC_{Rho}$ (with coiled-coil domain), which are monomeric in solution and surprisingly both catalytically active. Substituting Mg^{2+} for Mn^{2+} significantly increased activity for GC_{Rho} (330 fold), but not $GCwCC_{Rho}$ (1.4 fold). In addition, the presence of the coiled-coil domain decreased overall activity (21 fold) in the presence of Mn^{2+}, but increased overall activity (11 fold) in the presence of Mg^{2+}. This is in agreement with earlier studies [65] suggesting that other domains of RhoGC modulate the activity of the cyclase domain, and has also been proposed for human GC-1 [42,43,63]. The structure of monomeric GC_{Rho} (Fig. 3f) is very similar to that of other guanylyl cyclase domains [40–43], as expected based on sequence identity (36–37% with human $\alpha\beta GC^{cat}$, Fig. 4). Crystallization trials in the presence of substrate analog ddGTP and Mn^{2+} yielded a homodimeric structure. Yet, ddGTP was not observed in the electron density and a disulfide bridge between the two subunits forced a non-canonical head-to-head conformation of the homodimer that is likely not biologically relevant. Interestingly, the $GCwCC_{Rho}$ protein did not show significant disulfide formation, suggesting that the presence of the coiled coil may promote a different conformation. This result is in agreement with previous studies [33] that showed that the coiled-coil domain plays a preponderant role in GC-1 dimer formation. Analytical ultracentrifugation and size exclusion chromatography showed the presence of monomeric and dimeric GC_{Rho} in solution when ddGTP and Mn^{2+} were added. However, in the absence of substrate analog and metal, both GC_{Rho} and $GCwCC_{Rho}$ were exclusively monomeric. The cyclase activity of GC_{Rho} was shown to be dependent on enzyme concentration, as observed previously [40], providing indirect evidence for transient catalytically active homodimers. However, contrary to what was reported for Cya2 [40], the activity of GC_{Rho}

does not reach a maximum, even at an enzyme concentration of 60 μM. We noted that the activity assays were performed in low salt, while the size exclusion chromatography, AUC, and crystallization experiments were performed at higher salt concentration. While this may seem a trivial difference, Rauch et al. had showed that Cya2 was monomeric at higher salt concentration, and dimeric at lower salt concentrations [40]. Therefore, we propose that the activity and oligomerization of GC_{Rho} are likely dependent on salt concentration. Experiments to verify this hypothesis are necessary. Regardless, from the data presented, the authors propose that GC_{Rho} has a much weaker dimerization affinity (60–80 μM) than other cyclases, including human $\alpha\beta GC^{cat}$. While Winger et al. had suggested a dimerization K_D of ~0.45 μM for $\alpha\beta GCcat$ [63], we found that human catalytic domains are purified as a mixture of monomers, homodimers, and heterodimers [43]. Our extensive mass spectrometry studies, unfortunately not taken into account in Kumar et al., showed that the catalytic domain heterodimerization K_D is much higher than previously thought (see section 3.5), and likely causes the difficulties in obtaining $\alpha\beta GC^{cat}$ crystals.

4. Structural determinants for catalytic activity

The structure of the active $\alpha\beta GC^{cat}$ structure has remained elusive. However, several studies have suggested how specific structural elements are involved in $\alpha\beta GC^{cat}$ transitioning from the open inactive conformation to the closed active state (Fig. 5).

4.1. Activating mutations

Only two mutations have been reported to significantly increase basal GC-1 activity and both are located at or near the $\alpha\beta GC^{cat}$ dimer interface [55,56,59]. First, the αCys595Ser mutation showed a 3.8-fold increased basal activity over wild-type [55], mainly due to increased GTP affinity (10-fold lower K_m) [56]. The authors suggested that the mutation allowed GC-1 to increase catalytic activity through a conformational rearrangement similar to that induced by Mn^{2+} substitution. Based on our structure of wild-type $\alpha\beta GC^{cat}$ and activity measurements with Mg^{2+} and Mn^{2+} [43], we postulated that the thiol-to-hydroxyl substitution in the αCys595Ser mutant enhances hydrogen bonding with nearby residues αGlu526 and βThr474, promoting a reorientation of the residues at the dimer interface leading to an increase in basal cGMP output (Fig. 3g). This hypothesis is supported by earlier studies showing that αCys595Asp, αCys595Tyr, and αGlu526Ala mutations all resulted into significantly reduced basal and NO-stimulated activity [59,61] (see section 4.2), suggesting these residues may be involved in crucial inter-subunit contact. However, in the case of the αCys595 residue, we cannot rule out the role of Cys oxidation or potential Cys-S-NO modifications (see section 4.3). Finally, other studies have also proposed that the αCys595 residue could participate in YC-1 stimulator [59] or ATP binding in the pseudo-symmetry site of the catalytic domain [66,67]. However, recent studies have unambiguously showed that stimulators bind to the βHNOX domain of GC-1 [12].

Second, the βMet537Asn mutation was designed based on the homologous mutation in AC (C2-Lys1014Asn). While the K_m value was unchanged, basal V_{max} increased 6.8-fold in the mutant enzyme [60]. In addition, stimulation by NO and YC-1 increased activity of the mutant enzyme 48.4 fold and 4.5 fold, respectively. Consequently, for the mutant enzyme,

both basal and NO-stimulated activity are significantly greater than those in wild-type GC-1 (5.9 fold and 3.7 fold, respectively). Similar to the aforementioned αCys595Ser mutation, Lamothe et al. postulated that the βMet537Asn mutation enhances interfacial interactions at the catalytic domain for improved basal activity (Fig. 4). Based on our structure of the human wild-type αβGC^{cat} (Fig. 3h), we speculated that the βMet537Asn mutated residue could potentially interact with αLys524 and αThr527 [43]. Other studies showed that the αLys524Ala mutation (see section 4.3) reduced heterodimerization (3 fold), as well as basal GC-1 activity (38 fold) [61], thus supporting our hypothesis regarding potential intersubunit contacts involving αLys524.

4.2. Inactivating mutations

Mutations in the catalytic domain that reduce basal and/or NO-stimulated activity have also aided in identifying regions in αβGC^{cat} crucial for cGMP turnover. These mutations are located in three main regions: (i) the active site, (ii) the inter-subunit interface near the β-flap, and (iii) the inter-subunit interface near the active site.

4.2.1. Mutations in the active site—The αAsp530Ala mutant had no detectable basal or NO-stimulated activity [61]. This is not surprising since αAsp530 is located on the β2-β3 substrate binding loop and is predicted to coordinate the Mg^{2+} ion based on sequence alignment with adenylyl cyclase (Table 1) and structural modeling based on metal-containing AC [42]. Another mutation in the active site showed decreased basal activity. Residue βCys541 has been implicated in substrate specificity [54]. Substitution with Ser decreased activity in the presence of Mg^{2+} [55,56]; however, in the presence of Mn^{2+}, βCys541Ser retained low catalytic activity and was responsive to NO similarly to wild-type GC-1 [55]. To test the putative role of this residue in substrate specificity, the βGlu473/βCys541 pair was mutated into the AC homologous Lys/Asp pair, resulting in conversion of GC-1 into an NO-responsive adenylyl cyclase with abolished GTP cyclase activity [54]. Finally, the double mutant βGly476Cys/βCys541Ser catalytic domain also showed little to no activity in the presence of Mg^{2+} [42], likely due to the βCys541Ser mutation.

4.2.2. The dimer interface near the β-flap—Two mutations near the β-flap showed impaired activity. The αAsp514Ala mutant had no detectable basal or NO-stimulated activity and showed significantly decreased heterodimerization [61]. The αLys524Ala mutation resulted in significantly decreased basal cyclase activity and NO-stimulated activity compared to wild type (38 fold and 13.3 fold lower, respectively). However, this mutant was still responsive to NO; while wild-type GC-1 was stimulated by NO 118-fold, the αLys524Ala mutant activity was increased 338-fold. These two residues are located on the dorsal side of αβGC^{cat}, near βMet537 (see section 4.1) and were predicted to interact with the βGC flap-wrap [43]. A third mutation was recently identified in one individual diagnosed with achalasia, hypertension and Moyamoya disease [68]. The purified αCys517Tyr mutant showed decreased basal and NO-stimulated activities (see section 4.3 for details). The bulky Tyr could lead to structural disruption in the αGC^{cat} subunit near the interfacial βGC flap-wrap. Collectively, these studies suggest a crucial role for the βGC

flap-wrap not just for heterodimerization and proper orientation of the catalytic subunits crucial for basal activity, but also for NO signal transduction.

4.2.3. Mutations in the interfacial region near the active site—Several mutations located near the active site have also been shown to decrease GC-1 activity. First, the αGlu526Ala mutation resulted in significantly decreased basal and NO-stimulated cyclase activity (16 fold and 7 fold, respectively) compared to wild type [61]. The αGlu526 residue is located at the intersubunit interface near the putative pseudo-symmetric pocket. It has been implicated in binding of inhibitors in the pseudo-symmetric site of GC-1 [66]. We had proposed that this residue is part of a triad of residues important for orienting the two subunits to promote optimal activity [43]. Residues αGlu526, αCys595, and βThr474 could form a network of hydrogen bonds at the dimer interface, similar to the C1a-Lys436/C1a-Asp505/C2a-Thr939 triad in adenylyl cyclase [69]. This hypothesis is supported by previous mutagenesis studies that abrogate potential hydrogen bonds, including αCys595Asp, αCys595Tyr, and αCys595Asp/αGlu526Ala [59]. More recently, Agullo et al. recently proposed that αGlu526 interacts with αArg593 and β-flap residue βMet537 [70].

Second, the βAsp477Ala mutation showed lower NO- and YC-1-stimulated activity compared to wild-type GC-1, but a higher level of synergy between the two stimulators [59]. This residue is located near the putative pseudo-symmetric pocket that lacks key catalytic residues [42,71]. This site was proposed to bind nucleotides that would regulate the activity of the catalytic site [66]. A subsequent study suggested that this residue may be important for binding metal ions in the pseudo-symmetric site of GC-1 [66]. In contrast, the double mutant αCy-s595Ala/βAsp477Ala showed similar or slightly higher activity compared to wild-type GC-1 [72]. It was proposed that these residues play a key role in the communication between the two sites, specifically in the presence of excess NO, suggesting a link between NO and nucleotide regulation of GC-1 activity.

Third, mutation of αCys595 into Tyr significantly decreased basal and stimulated activity (2.8 fold and 2.1 fold, respectively). However, the αCys595Tyr mutant protein was synergistically activated by NO and YC-1 to a greater extent than wild type (1.8 fold more). Decreased activity stems from both an increase in K_m and a decrease in V_{max} [59]. The remarkable opposite effects of the αCys595Ser (see section 4.1) and αCys595Tyr mutations on basal activity suggested that this residue is important for catalysis, despite not being part of the catalytic site. It was originally proposed that this residue is involved in YC-1 binding, but recent studies have shown that stimulators bind to the βHNOX sensor domain instead [12]. Instead, we proposed that αCys595 is part of a network of interfacial hydrogen bonds that promote an optimal orientation of both subunits for high catalytic activity [43].

4.3. Cys-NO modification in GC-1 desensitizes the enzyme to NO

S-nitrosation (S-NO) is a well-recognized post-translational modification of Cys residues that regulates a myriad of pathways [73]. Approximately 3% of GC-1 amino acids are Cys, almost twice the average amount found in globular proteins [74]. Multiple roles for S-NO modified GC-1 have been speculated, including enhanced NO-stimulation [27,28]

or reduced cGMP output, possibly representing a state of oxidative stress [75]. However, the stability of nitrosothiols has also been questioned given the millimolar concentrations of cellular reductants such as glutathione [76–78], calling into question the significance of S-NO modified GC-1. While the precise role of this posttranslational modification remains under debate, there are several functions that S-NO may have in tuning GC-1 activity and how $\alpha\beta GC^{cat}$ may be affected.

NO desensitization of GC-1 is characterized by a loss of sensitivity for NO and was shown to occur via S-NO modification of GC-1 Cys residues in primary artery smooth muscle cells treated with S-nitrosocysteine [75]. Pre-treatment of smooth muscle cells with a glutathione precursor reduced levels of S-NO modified GC-1 and restored NO-sensitivity. Two Cys residues were found to be posttranslationally S-NO modified, αCys243 and βCys122 [75]. Fernhoff et al. reported S-NO to be involved in reductive nitrosylation of ferric heme and identified two Cys residues, βCys78 or βCys122, acting as nucleophiles in the reaction. Reductive nitrosylation reduces oxidized heme iron using one NO molecule and a nucleophilic base to regenerate the NO-sensitive ferrous heme. Finally, thiol alkylation prevented recovery of NO-sensitivity while DTT treatment rescued ferrous heme, suggesting that reduced Cys residues are crucial for maintaining NO-sensitive GC-1 [31,79]. However, it has been reported that the NO-modified GC-1 Cys residues are not canonical S-NO modifications [31]. Instead, the authors suggested a radicalized S-NO with the loss of a single electron.

Additional Cys residues modified by S-nitrosation have recently been identified [80]. Using a combination of the biotin switch assay (BST) and Orbitrap tandem mass spectrometry, Beuve et al. enhanced the detection limit of S-NO modifications and identified ten conserved Cys residues as S-NO targets, including six Cys localized to the $\alpha\beta GC^{cat}$ catalytic domains: αCys517, αCys595, αCys610, αCys629, βCys541, and βCys571. These results suggest a potential role for S-NO post-translational modifications in regulating catalytic activity. The αCys595 and βCys541 residues have been shown to play major roles in catalytic activity (see sections 4.1 and 4.2). Residues αCys629 and βCys571 are located away from the active site and subunit interface, and their role is not clear. Residue αCys609, was reported to be involved in a direct interaction between GC-1 and thioredoxin (Trx; see section 5.2) [30]. Finally, the αCys517 residue has been reported by two separate groups to be involved in GC-1 activity and NO-sensitivity. Crassous et al. first reported that αCys517 mediates GC-1 desensitization to NO in angiotensin II-induced hypertension [81]. Another study revealed the presence of an αCys517 mutant in a subject presenting Moyamoya disease (MMD). MMD is characterized by aberrant arterial remodeling in the brain leading to thrombosis and hemorrhage and has been associated with a dysfunctional GC-1 [82]. Wallace et al. identified the αCys517Tyr variant in a subject with diagnosed MMD [68]. *In vitro* NO response curves of the GC-1 αCys517Tyr mutant indicated a 60% loss of NO-sensitivity, in good agreement with results from Crassous et al. Collectively, these results suggest that S-NO modifications of Cys residues could lead to dramatic reduction in GC-1 activity and activation. While the stability and relevance of S-NO modifications is controversial due to the reducing environment in cells, it has been shown that these modifications are specific and controlled mainly by cysteine reactivity and their surrounding microenvironment [76,78]. These results suggest that S-NO modifications of GC-1 Cys

residues are biologically relevant, but that the exact function of these Cys modifications remain to be determined (reviewed in Ref. [74]).

4.4. Small molecules targeting the catalytic domain

Identification of small molecules that bind to and activate $\alpha\beta GC^{cat}$ could lead to a novel class of heme-independent GC-1 activators. Cobinamide, a precursor to the biosynthesis of vitamin B_{12}, was found to activate GC-1 independent of heme oxidation [83]. With known GC-1 stimulator BAY 41-2272, cobinamide synergistically enhanced cGMP output and approached maximum NO-stimulated activity. Deletion of the $\alpha\beta$HNOX domains had no effect on cobinamide sensitivity, supporting the hypothesis that binding could occur in the catalytic domain. Further structural studies and activity measurements using the isolated catalytic domain are necessary to define the binding site for cobinamide and how it could promote activity. Derivatives of YC-1 have been synthesized and screened using surface plasmon resonance (SPR) to determine binding to immobilized $\alpha\beta GC^{cat}$ [84]. SPR measurements identified several small molecules with YC-1 modifications that could bind to the catalytic domain and increase activity. However, because purified $\alpha\beta GC^{cat}$ consists of a mixture of monomers, heterodimers, and homodimers [43], it is unclear whether the reported small molecules do indeed target the catalytically-competent heterodimer.

Inhibition of GC-1 may seem counterintuitive, but several groups have targeted GC-1 in cases of migraines [85], septic shock [86], cancer [87,88], and neurological disorders such as Parkinson's Disease [89]. Structural characterization of the inhibited C1/C2 adenylyl cyclase domain has alluded to key structural elements involved in domain activation, which could be applied to $\alpha\beta GC^{cat}$. Nucleotide-based small molecules with $2',3'-O$-(2,4,6-trinitrophenyl) (TNP)- or $2',3'-O$-(N-me-thylanthraniloyl) (MANT)-substitutions at the NTP ribosyl ring display nanomolar affinity for GC-1 [90–93] and are predicted to bind in the GTP-binding cleft in $\alpha\beta GC^{cat}$. Crystal structures of C1/C2 bound to either TNP-ATP, MANT-ATP or MANT-GTP were subsequently solved and used to identify key interactions between the inhibitor and cyclase subunits [94]. These results confirmed that MANT/TNP binding occurred in the hydrophobic pocket and showed several ionic interactions between the NO_2 groups of TNP and Asn1022 and Asn1025 from the C2 subunit. Structural comparison between the three inhibitors also highlighted a highly plastic dimer interface that can accommodate different nucleobases. These studies suggested that inhibitor binding traps the catalytic domain in a competent, but inhibited, conformation.

Dove *et al.* expanded on how this class of competitive inhibitors could be used to target the active $\alpha\beta GC^{cat}$ domain [93]. TNP-ATP, TNP-GTP, and $2'$-MANT-$3'$-dATP were shown to potently inhibit GC-1 with K_i of 7.3 nM, 8.6 nM, and 16.7 nM respectively. Molecular modeling using the mutant $\alpha\beta GC^{cat}$ crystal structure (PDB code 3UVJ) and docking with $2'$-MANT-$3'$-dATP supported the theory that inhibitor binding could induce partial domain closure including a 27° rotation of αGC around βGC as previously proposed [41–43]. While complete domain closure is not possible due to the bulky MANT/TNP moiety, these inhibitors could be ideal for targeting the activated $\alpha\beta GC^{cat}$ domain due to their high affinity and increased fluorescence upon binding.

Recently, several groups have synthesized non nucleotide-based small molecules that reportedly bind to αβGC^{cat} with μM affinity. Mota et al. identified quinoxaline-based small molecules with a K_D of 11 μM [95]. Activity assays using GC-1, GTP and activator cinaciguat suggested these molecules inhibit active GC-1, but do not compete with substrate binding. Molecular modeling suggested binding to the supposed pseudo-symmetric site. However, earlier studies by the same group proposed binding of YC-1 to the catalytic domain [84], in contrast to the recent studies showing that these stimulators bind to the βHNOX domain [12]. Therefore, the exact binding site of these inhibitors remains elusive.

In silico screening was performed using the αβGC^{cat} crystal structure (PDB code 3UVJ) to discover inhibitors that bind in the pseudo-symmetric pocket [96]. Two molecules were shown to inhibit basal and NO- stimulated GC-1 with K_i of ~20–30 μM. Only one of the two compounds was capable of inhibiting the isolated catalytic domains, albeit with severely diminished potency; 100 μM was used to inhibit 99% GC-1 activity while 400 μM inhibited > 50% of activity using αβGC^{cat}. Regardless, the determination of the exact binding site of these molecules awaits structural characterization.

5. Protein-protein interactions regulating GC-1 activity

5.1. βHNOX-αβGC^{cat} interactions

Despite the determination of low-resolution electron-microscopy structures of GC-1 [39], the mechanism by which NO regulates its activity remains unknown. One hypothesis is that direct interaction between αβGC^{cat} and βHNOX transduces the signal of NO-stimulation. Several groups aimed to test this mechanism. This hypothesis was first suggested by Winger et al. [63], who showed that increasing molar equivalents of βHNOX or βHNOX-PAS and most of the CC domain (β385) added to αβGC^{cat} yielded stepwise decreases in catalytic activity [63]. However, two observations raised questions about a possible interaction between the two domains: a large molar excess of βHNOX-PAS compared to αβGC^{cat} (15:1) was necessary to elicit a ~55% decrease in activity, and adding NO had no effect on inhibition. Regardless, the authors suggested that βHNOX could act as an autoinhibitory element on GC-1 activity. Another study further supported a possible interaction between the N-terminal domains and the C-terminal catalytic domains. Förster resonance energy transfer (FRET) analysis of fluorescent fusion proteins showed the proximity of the HNOX domains and the catalytic domain [97]. Importantly, fusion of the large fluorescent proteins (YFP and CFP) to GC-1 did not affect its basal or stimulated activity. However, NO binding had no effect on FRET efficiency, as observed previously, suggesting that this potential interaction between βHNOX and αβGC^{cat} is independent of NO binding. A recent study using C-terminally tagged CFP-tagged αGC-1 and YFP-tagged βGC-1 polypeptides showed a modest increase in FRET efficiency (~10%) upon NO-donor addition, which would support domain closure and tighter interactions between αGC^{cat} and βGC^{cat}. Adding GTP slightly reduced FRET efficiency by ~7%, which could indicate opening of the substrate binding pocket. However, none of the *in vitro* or *in vivo* fluorescence measurements recorded by Pan et al. were correlated to GC-1 activity [98]. Adding NO had no effect on FRET efficiency when using CFP-αGC-1 (N-terminally tagged) and βGC-1-YFP (C-terminally tagged), in agreement with previous studies [97].

Busker et al. were the first to report NO-induced alterations in interactions between βHNOX and αβGC^{cat}. Endogenous Trp residues located in βHNOX (Trp22), βGC^{cat} (Trp602), αPAS (Trp352), αCC (Trp466), and αGC^{cat} (Trp669) were used as FRET donors, and MANT-dGTP bound to the catalytic domain was used as a FRET acceptor [99]. While the low quantum yield of Trp residues make them suboptimal FRET partners [100], changes in FRET efficiency were observed in this study. In wild-type GC-1, FRET efficiency increased 155% upon NO stimulation, while the αCC Trp466Phe mutation reduced FRET efficiency compared to wild-type GC-1. This suggests that Trp466 may be involved in NO-induced signal transduction. By retaining Trp22 in βHNOX and Trp466 as the only FRET donors, FRET efficiency increased to 200% upon addition of NO, suggesting that these two Trp moved closer to the MANT-GTP molecule. Busker et al. concluded that domains docking onto αβGC^{cat} lead to low activity. NO binding induces a conformational rearrangement in the heme pocket that is carried directly to αβGC^{cat} via Trp22 in βHNOX as well as indirectly through the PAS and CC domains via Trp466 in αCC to promote an active conformation of the catalytic domain.

Hydrogen-Deuterium Exchange Mass Spectrometry (HDXMS) studies have further supported a model where βHNOX interacts directly with the αβGC^{cat} domain. The first study mapped interactions between the βHNOX-PAS construct and the αβGC^{cat} domain [58]. The αβGC^{cat} domain exhibit decreased deuterium incorporation mostly in the C-terminal lobe (residues 601-655) of αGC^{cat} in the presence of βHNOX-PAS compared to the catalytic domain alone. The decreased deuterium incorporation in that region of αβGC^{cat} was also observed in the context of full-length GC-1, suggesting that this region could be involved in interactions with βHNOX-PAS. The C-terminal region of βGC^{cat} (residues 568-604) also showed decreased deuterium incorporation in the presence of βHNOX-PAS, but this was not observed in the context of full-length GC-1. These results suggest that the C-terminal region of αGC^{cat} could be involved in direct interactions with the N-terminal sensor domain of GC-1 (Fig. 4). This model is supported by the fact that this region presents high sequence conservation [43], and studies showing that the αArg624Ala mutation in that region drastically reduced GC-1 activity [61]. Another study by the same group showed that NO addition to full-length GC-1 resulted in changes in H/D exchange rates in all domains of GC-1 [101]. In the catalytic domains, the substrate-binding loop of αGC^{cat} (region 522-532) and the β-flap wrap (region 586-593) showed decreased exchange, while the substrate-binding loop of βGC^{cat} (residues 469-482) showed increased exchange. The α-helices that "cap" the active site in both subunits (α599-610 and β545-556) showed decreased deuterium incorporation, suggesting an overall "closing" of the active site. In addition, subtle decreased exchange in the C-terminal lobe of αGC^{cat} and βGC^{cat} was also observed. Ultimately, these studies show that subtle rather than large conformational changes distributed along the GC-1 polypeptide seem to be part of the activation mechanism by NO (Fig. 5). This mechanism was further supported by electron microscopy studies that showed that GC-1 shows a high degree of flexibility [39]. This study confirmed previous results suggesting that the coiled-coil domains act as a scaffold and provide two pivot points for other GC-1 domains to move [37]. GC-1 assembles in a continuous range of conformations, with the two extremes corresponding to an extended conformation and a collapsed conformation. In the extended conformation, the αβGC^{cat} and the αβHNOX-PAS

domains are located on either end of the extended coiled-coil domain. In the collapsed conformation, the αβHNOX-PAS is folded on the coiled-coil domain with the βHNOX in close proximity to the catalytic domain. Interestingly, adding NO, a non-cyclizable GTP analog, or both did not significantly alter the range of conformations adopted by GC-1.

Taken together, results from these complementary studies suggest that NO-stimulation of GC-1 is not a simple on-off switch where, in the absence of NO, βHNOX maintains αβGC^{cat} in an inactive conformation through a direct interaction and, upon NO binding to heme, βHNOX is released and optimal catalytic activity can occur. Instead, NO-stimulation may trigger subtle changes in conformations and interactions across each domain that orient αβGC^{cat} in an optimal conformation for catalysis (Fig. 5).

5.2. Interactions with thioredoxin (Trx)

Trx is typically known to mediate disulfide bonds but can also denitrosylate S-NO residues, suggesting Trx may act as a switch in sensitizing and desensitizing GC-1 to NO. Co-expression of GC-1 and Trx improved NO-stimulated GC-1 activity (~2-fold) while inhibition of activated Trx led to an increased amount of S-NO modified GC-1 and significantly decreased NO-sensitivity [30]. Using a proximity ligation assay and immunoprecipitation, Trx was found to associate primarily with αGC-1 via a disulfide linkage with αCys609. Molecular docking using structures of Trx and αβGC^{cat} (PDB code 4NI2) suggested Trx docks onto the C-terminal lobe of αGC^{cat}, very close to the substrate-binding groove, to mediate S-NO modifications on GC-1. The authors proposed that Trx binding could compete with HNOX binding to the catalytic domain or de-nitrosate other GC-1 residues. The mechanism of Trx-induced protection of GC-1 activity remains to be determined.

5.3. Interactions with protein-disulfide isomerase (PDI)

Protein-disulfide isomerase (PDI) assists in protein folding by catalyzing disulfide bond formation and breakage using a Cys-X-X-Cys motif in its active site. An interaction between PDI and GC-1 was reported using a GC-1 affinity matrix [102]. Non-reducing gel electrophoresis and immunoprecipitation indicated this interaction is redox-controlled [103]. Comparing basal and NO-stimulated GC-1 activities in the presence of PDI found that PDI primarily targets NO-stimulated GC-1, reducing NO-stimulated activity by 41%. Using amine linkage and tandem mass spectrometry previously employed to cross-link Lys residues in GC-1 and identify domain-domain interactions [37], Heckler et al. found cross-links between PDI and GC-1 residue αLys672 and βLys615, both located on disordered C-terminal regions not visible in the crystal structures of αβGC^{cat} [104]. Truncations of GC-1 indicated PDI preferentially interacts with the αGC^{cat} subunit. Molecular dynamics studies suggested that PDI could interact with αGC^{cat} to prevent NO-activation in a fashion similar to βHNOX. Together, these results hint at a redox-dependent interaction between the catalytic domain of GC-1 and PDI through a disulfide linkage.

6. Conclusions

Much progress has been made toward characterizing NO-stimulated GC-1, but we still lack a mechanistic understanding of how αβGC^{cat} transitions between inactive and active forms in the full-length enzyme. Structural studies of GC catalytic domains from different organisms and the C1/C2 domain from AC have aided in identifying catalytic residues, potential allosteric sites for small molecules, and regions in the catalytic domain possibly involved in protein-protein interactions either with other GC-1 domains or other protein partners. Determination of the activated αβGC^{cat} conformation will expand on small molecules that can target αβGC^{cat}. These small molecules will aid, not only in structural studies aimed at characterizing the catalytic domain, but in creating a novel class of pharmaceuticals to target GC-1 independent of the NO-sensor domain. Further studies are required to determine what role βHNOX plays in regulating αβGC^{cat} and to identify additional protein-protein interaction partners that assist GC-1. While we still lack a high-resolution structure of GC-1, this should not impede progress in the field, but rather drive researchers to utilize alternative methods toward understanding and targeting dysfunctional GC-1 in a variety of diseases.

Acknowledgments

Abbreviations

GC-1	Soluble guanylyl cyclase
AC	adenylyl cyclase
GC$_{cya2}$	*Synechocystis PCC 6803* Cya2 guanylyl cyclase domain
GC$_{Cr}$	*C. reinhardtii* guanylyl cyclase domain
αβ GC^{cat}	human GC-1 catalytic domain
GC$_{Rho}$	*B. emersonii* guanylyl cyclase domain
S-NO	S-nitrosation

References

1. Derbyshire ER, Marletta MA. Structure and regulation of soluble guanylate cyclase. Annu Rev Biochem. 81 2012; :533–559. DOI: 10.1146/annurev-biochem-050410-100030 [PubMed: 22404633]

2. Montfort WR, Wales JA, Weichsel A. Structure and activation of soluble guanylyl cyclase, the nitric oxide sensor. Antioxidants Redox Signal. 26 2016; :107–121. DOI: 10.1089/ars.2016.6693

3. Lundberg JO, Gladwin MT, Weitzberg E. Strategies to increase nitric oxide signalling in cardiovascular disease. Nat Rev Drug Discov. 14 2015; :623–641. DOI: 10.1038/nrd4623 [PubMed: 26265312]

4. Buys ES, Potter LR, Pasquale LR, Ksander BR. Regulation of intraocular pressure by soluble and membrane guanylate cyclases and their role in glaucoma. Front Mol Neurosci. 7 2014; :1–15. DOI: 10.3389/fnmol.2014.00038 [PubMed: 24574959]

5. Fritz BG, Hu X, Brailey JL, Berry RE, Walker FA, Montfort WR. Oxidation and loss of heme in soluble guanylyl cyclase from Manduca sexta. Biochemistry. 50 2011; :5813–5815. DOI: 10.1021/bi200794c.Oxidation [PubMed: 21639146]

6. Stasch J, Schmidt PM, Nedvetsky PI, Nedvetskaya TY, AKHS, Meurer S, Deile M, Taye A, Knorr A, Lapp H, Müller H, Turgay Y, Rothkegel C, Tersteegen A, Kemp-Harper B, Müller-Esterl W, Schmidt HHHW. Targeting the heme-oxidized nitric oxide receptor for selective vasodilatation of diseased blood vessels. J Clin Invest. 116 2006; :2552–2561. DOI: 10.1172/JCI28371DS1 [PubMed: 16955146]

7. Follmann M, Griebenow N, Hahn MG, Hartung I, Mais FJ, Mittendorf J, Schäfer M, Schirok H, Stasch JP, Stoll F, Straub A. The chemistry and biology of soluble guanylate cyclase stimulators and activators. Angew Chem Int Ed Engl. 52 2013; :9442–9462. DOI: 10.1002/anie.201302588 [PubMed: 23963798]

8. Ghofrani HA, D'Armini AM, Grimminger F, Hoeper MM, Jansa P, Kim NH, Mayer E, Simonneau G, Wilkins MR, Fritsch A, Neuser D, Weimann G, Wang C. Riociguat for the treatment of chronic thromboembolic pulmonary hypertension. N Engl J Med. 369 2013; :319–329. DOI: 10.1056/NEJMoa1209657 [PubMed: 23883377]

9. Martin F, Baskaran P, Ma X, Dunten PW, Schaefer M, Stasch JP, Beuve A, van den Akker F. Structure of cinaciguat (BAY 58-2667) bound to Nostoc H-NOX domain reveals insights into heme-mimetic activation of the soluble guanylyl cyclase. J Biol Chem. 285 2010; :22651–22657. DOI: 10.1074/jbc.M110.111559 [PubMed: 20463019]

10. Gheorghiade M, Greene SJ, Filippatos G, Erdmann E, Ferrari R, Levy PD, Maggioni A, Nowack C, Mebazaa A. Cinaciguat, a soluble guanylate cyclase activator: results from the randomized, controlled, phase IIb COMPOSE programme in acute heart failure syndromes. Eur J Heart Fail. 14 2012; :1056–1066. DOI: 10.1093/eurjhf/hfs093 [PubMed: 22713287]

11. Zhou Z, Pyriochou A, Kotanidou A, Dalkas G, van Eickels M, Spyroulias G, Roussos C, Papapetropoulos A. Soluble guanylyl cyclase activation by HMR-1766 (ataciguat) in cells exposed to oxidative stress. Am J Physiol Heart Circ Physiol. 295 2008; :H1763–H1771. DOI: 10.1152/ajpheart.51.2008 [PubMed: 18757489]

12. Wales, JA; Chen, C-Y; Breci, L; Weichsel, A; Bernier, SG; Sheppeck, JE; Solinga, R; Nakai, T; Renhowe, PA; Jung, J; Montfort, WR. Discovery of stimulator binding to a conserved pocket in the heme domain of soluble guanylyl cyclase. J Biol Chem. 2017.

13. Altan-Yaycioglu R, Türker G, Akdöl S, Acuna G, Izgi B. The effects of beta-blockers on ocular blood flow in patients with primary open angle glaucoma: a color Doppler imaging study. Eur J Ophthalmol. 11 2001; :37–46. DOI: 10.1177/112067210101100108 [PubMed: 11284483]

14. Kee C, Kaufman PL, Gabelt BT. Effect of ticrynafen on aqueous humor dynamics in monkeys. Arch Ophthalmol. 35 1994; :2769–2773.

15. Kotikoski H, Alajuuma P, Moilanen E, Salmenperä P, Oksala O, Laippala P, Vapaatalo H. Comparison of nitric oxide donors in lowering intraocular pressure in rabbits: role of cyclic GMP. J Ocul Pharmacol Therapeut. 18 2002; :11–23. DOI: 10.1089/108076802317233171

16. Buys ES, Ko YC, Alt C, Hayton SR, Jones A, Tainsh LT, Ren R, Giani A, Clerté M, Abernathy E, Tainsh RET, Oh DJ, Malhotra R, Arora P, de Waard N, Yu B, Turcotte R, Nathan D, Scherrer-Crosbie M, Loomis SJ, Kang JH, Lin CP, Gong H, Rhee DJ, Brouckaert P, Wiggs JL, Gregory MS, Pasquale LR, Bloch KD, Ksander BR. Soluble guanylate cyclase α1–deficient mice: a novel murine model for primary open angle glaucoma. PLoS One. 8 2013; doi: 10.1371/journal.pone.0060156

17. Ge P, Navarro ID, Kessler MM, Bernier SG, Perl NR, Sarno R, Masferrer J, Hannig G, Stamer WD. The soluble guanylate cyclase stimulator IWP-953 increases conventional outflow facility in mouse eyes. Investig Ophthalmol Vis Sci. 57 2016; :1317–1326. DOI: 10.1167/iovs.15-18958 [PubMed: 26998718]

18. Stasch JP, Schlossmann J, Hocher B. Renal effects of soluble guanylate cyclase stimulators and activators: a review of the preclinical evidence. Curr Opin Pharmacol. 21 2015; :95–104. DOI: 10.1016/j.coph.2014.12.014 [PubMed: 25645316]

19. Wang Y, Krämer S, Loof T, Martini S, Kron S, Kawachi H, Shimizu F, Neumayer HH, Peters H. Enhancing cGMP in experimental progressive renal fibrosis: soluble guanylate cyclase stimulation vs. phosphodiesterase inhibition. Am J Physiol Ren Physiol. 290 2006; :F167–F176. DOI: 10.1152/ajprenal.00197.2005

20. Hoffmann LS, Kretschmer A, Lawrenz B, Hocher B, Stasch JP. Chronic activation of heme free guanylate cyclase leads to renal protection in dahl salt-sensitive rats. PLoS One. 10 2015; :1–17. DOI: 10.1371/journal.pone.0145048

21. Ito K, Chen J, Seshan SV, Khodadadian JJ, Gallagher R, El Chaar M, Vaughan E, Poppas DP, Felsen D. Dietary arginine supplementation attenuates renal damage after relief of unilateral ureteral obstruction in rats. Kidney Int. 68 2005; :515–528. DOI: 10.1111/j.1523-1755.2005.00429.x [PubMed: 16014028]

22. Russwurm M, Behrends S, Harteneck C, Koesling D. Functional properties of a naturally occurring isoform of soluble guanylyl cyclase. Biochemistry. 335 1998; :125–130.

23. Plate L, Marletta MA. Nitric oxide-sensing H-NOX proteins govern bacterial communal behavior. Trends Biochem Sci. 38 2013; :566–575. DOI: 10.1016/j.tibs.2013.08.008 [PubMed: 24113192]

24. Purohit R, Fritz BG, The J, Issaian A, Weichsel A, David CL, Campbell E, Hausrath AC, Rassouli-Taylor L, Garcin ED, Gage MJ, Montfort WR. YC-1 binding to the β subunit of soluble guanylyl cyclase overcomes allosteric inhibition by the α subunit. Biochemistry. 53 2014; :101–114. DOI: 10.1021/bi4015133 [PubMed: 24328155]

25. Zhao Y, Schelvis JP, Babcock GT, Marletta MA. Identification of histidine 105 in the beta1 subunit of soluble guanylate cyclase as the heme proximal ligand. Biochemistry. 37 1998; :4502–4509. DOI: 10.1021/bi972686m [PubMed: 9521770]

26. Zhao Y, Brandish PE, Ballou DP, Marletta MA. A molecular basis for nitric oxide sensing by soluble guanylate cyclase. Proc Natl Acad Sci Unit States Am. 96 1999; :14753–14758. DOI: 10.1073/pnas.96.26.14753

27. Ibrahim M, Derbyshire ER, Soldatova AV, Marletta MA, Spiro TG. Soluble guanylate cyclase is activated differently by excess NO and by YC-1: resonance Raman spectroscopic evidence. Biochemistry. 49 2010; :4864–4871. DOI: 10.1021/bi100506j [PubMed: 20459051]

28. Russwurm M, Koesling D. NO activation of guanylyl cyclase. EMBO J. 23 2004; :4443–4450. DOI: 10.1038/sj.emboj.7600422 [PubMed: 15510222]

29. Martin E, Berka V, Sharina I, Tsai AL. Mechanism of binding of NO to soluble guanylyl cyclase: implication for the second NO binding to the heme proximal site. Biochemistry. 51 2012; :2737–2746. DOI: 10.1021/bi300105s [PubMed: 22401134]

30. Huang C, Alapa M, Shu P, Nagarajan N, Wu C, Sadoshima J, Kholodovych V, Li H, Beuve A. Guanylyl cyclase sensitivity to nitric oxide is protected by a thiol oxidation-driven interaction with thioredoxin-1. J Biol Chem. 292 2017; :14362–14370. DOI: 10.1074/jbc.M117.787390 [PubMed: 28659344]

31. Fernhoff NB, Derbyshire ER, Marletta MA. A nitric oxide/cysteine interaction mediates the activation of soluble guanylate cyclase. Proc Natl Acad Sci U S A. 106 2009; :21602–21607. DOI: 10.1073/pnas.0911083106 [PubMed: 20007374]

32. Guo Y, Suess DLM, Herzik MA, Iavarone AT, Britt RD, Marletta MA. Regulation of nitric oxide signaling by formation of a distal receptor-ligand complex. Nat Chem Biol. 13 2017; :1216–1221. DOI: 10.1038/nchembio.2488 [PubMed: 28967923]

33. Ma X, Sayed N, Baskaran P, Beuve A, van den Akker F. PAS-mediated dimerization of soluble guanylyl cyclase revealed by signal transduction histidine kinase domain crystal structure. J Biol Chem. 283 2008; :1167–1178. DOI: 10.1074/jbc.M706218200 [PubMed: 18006497]

34. Purohit R, Weichsel A, Montfort WR. Crystal structure of the Alpha subunit PAS domain from soluble guanylyl cyclase. Protein Sci. 22 2013; :1439–1444. DOI: 10.1002/pro.2331 [PubMed: 23934793]

35. Sarkar, A; Dai, Y; Haque, MM; Seeger, F; Ghosh, A; Garcin, ED; Montfort, WR; Hazen, SL; Misra, S; Stuehr, DJ. Heat shock protein 90 associates with the per-arnt-sim domain of heme-free soluble guanylate cyclase: implications for enzyme maturation. J Biol Chem. 2015.

36. Ma X, Beuve A, van den Akker F. Crystal structure of the signaling helix coiled-coil domain of the beta1 subunit of the soluble guanylyl cyclase. BMC Struct Biol. 10 2010; :2. doi: 10.1186/1472-6807-10-2 [PubMed: 20105301]

37. Fritz BG, Roberts SA, Ahmed A, Breci L, Li W, Weichsel A, Brailey JL, Wysocki VH, Tama F, Montfort WR. Molecular model of a soluble guanylyl cyclase fragment determined by small-angle X-ray scattering and chemical cross-linking. Biochemistry. 52 2013; :1568–1582. DOI: 10.1021/bi301570m [PubMed: 23363317]

38. Rothkegel C, Schmidt PM, Atkins DJ, Hoffmann LS, Schmidt HHHW, Schröder H, Stasch JP. Dimerization region of soluble guanylate cyclase characterized by bimolecular fluorescence complementation in vivo. Mol Pharmacol. 72 2007; :1181–1190. DOI: 10.1124/mol.107.036368 [PubMed: 17715400]

39. Campbell MG, Underbakke ES, Potter CS, Carragher B, Marletta MA. Single-particle EM reveals the higher-order domain architecture of soluble guanylate cyclase. Proc Natl Acad Sci Unit States Am. 111 2014; :2960–2965. DOI: 10.1073/pnas.1400711111

40. Rauch A, Leipelt M, Russwurm M, Steegborn C. Crystal structure of the guanylyl cyclase Cya2. Proc Natl Acad Sci U S A. 105 2008; :15720–15725. DOI: 10.1073/pnas.0808473105 [PubMed: 18840690]

41. Winger JA, Derbyshire ER, Lamers MH, Marletta MA, Kuriyan J. The crystal structure of the catalytic domain of a eukaryotic guanylate cyclase. BMC Struct Biol. 8 2008; doi: 10.1186/1472-6807-8-42

42. Allerston CK, von Delft F, Gileadi O. Crystal structures of the catalytic domain of human soluble guanylate cyclase. PLoS One. 8 2013; :1–9. DOI: 10.1371/journal.pone.0057644

43. Seeger F, Quintyn R, Tanimoto A, Williams GJ, Tainer JA, Wysocki VH, Garcin ED. Interfacial residues promote an optimal alignment of the catalytic center in human soluble guanylate cyclase: heterodimerization is required but not sufficient for activity. Biochemistry. 53 2014; :2153–2165. DOI: 10.1021/bi500129k [PubMed: 24669844]

44. Kumar RP, Morehouse BR, Fofana J, Trieu MM, Zhou DH, Lorenz MO, Oprian DD. Structure and monomer/dimer equilibrium for the guanylyl cyclase domain of the optogenetics protein RhoGC. J Biol Chem. 292 2017; :21578–21589. DOI: 10.1074/jbc.M117.812685 [PubMed: 29118188]

45. Smigel MD. Purification of the catalyst of adenylate cyclase. J Biol Chem. 261 1986; :1976–1982. [PubMed: 3080431]

46. Zhang G, Liu Y, Ruoho AE, Hurley JH. Structure of the adenylyl cyclase catalytic core. Nature. 386 1997; :247–253. [PubMed: 9069282]

47. Tesmer JJ, Sunahara RK, Gilman AG, Sprang SR. Crystal structure of the catalytic domains of adenylyl cyclase in a complex with Gs·GTPS. Science. 278 1997; :1907–1916. DOI: 10.1126/science.278.5345.1907 [PubMed: 9417641]

48. Sunahara RK. Isoforms of mammalian adenylyl cyclase: multiplicities of signaling. Mol Interv. 2 2002; :168–184. DOI: 10.1124/mi.2.3.168 [PubMed: 14993377]

49. Seifert R, Lushington GH, Mou T, Gille A, Sprang SR. Inhibitors of membranous adenylyl cyclases. Trends Pharmacol Sci. 33 2012; :64–78. DOI: 10.1086/498510.Parasitic [PubMed: 22100304]

50. Jaggupilli, A; Dhanaraj, P; Pritchard, A; Sorensen, JL; Dakshinamurti, S; Chelikani, P. Study of adenylyl cyclase-GαS interactions and identification of novel AC ligands. Mol Cell Biochem. 2018.

51. Pinto C, Papa D, Hubner M, Mou TC, Lushington GH, Seifert R. Activation and inhibition of adenylyl cyclase isoforms by forskolin analogs. J Pharmacol Exp Therapeut. 325 2008; :27–36. DOI: 10.1124/jpet.107.131904

52. Brand CS, Hocker HJ, Gorfe AA, Cavasotto CN, Dessauer CW. Isoform selectivity of adenylyl cyclase inhibitors: characterization of known and novel compounds. J Pharmacol Exp Therapeut. 347 2013; :265–275. DOI: 10.1124/jpet.113.208157

53. Ochoa de Alda JAG, Ajlani G, Houmard J. Synechocystis Strain PCC 6803 cya2,a prokaryotic gene theat encodes a guanylyl cyclase. J Bacteriol. 182 2000; :3839–3842. [PubMed: 10851002]

54. Sunahara RK, Beuve A, Tesmer JJG, Sprang SR, Garbers DL, Gilman AG. Exchange of substrate and inhibitor specificities between adenylyl and guanylyl cyclases. J Biol Chem. 273 1998; :16332–16338. [PubMed: 9632695]

55. Friebe A, Wedel B, Harteneck C, Foerster J, Schultz G, Koesling D. Functions of conserved cysteines of soluble guanylyl cyclase. Biochemistry. 36 1997; :1194–1198. DOI: 10.1021/bi962047w [PubMed: 9063867]

56. Friebe A, Russwurm M, Mergia E, Koesling D. A point-mutated guanylyl cyclase with features of the YC-1-stimulated enzyme: implications for the YC-1 binding site? Biochemistry. 38 1999; :15253–15257. [PubMed: 10563809]

57. Beste KY, Burhenne H, Kaever V, Stasch J, Seifert R. Nucleotidyl cyclase activity of soluble guanylyl cyclase $\alpha 1\beta 1$. Biochemistry. 51 2011; :194–204. DOI: 10.1021/bi201259y [PubMed: 22122229]

58. Underbakke ES, Iavarone AT, Marletta MA. Higher-order interactions bridge the nitric oxide receptor and catalytic domains of soluble guanylate cyclase. Proc Natl Acad Sci U S A. 110 2013; :6777–6782. DOI: 10.1073/pnas.1301934110 [PubMed: 23572573]

59. Lamothe M, Chang FJ, Balashova N, Shirokov R, Beuve A. Functional characterization of nitric oxide and YC-1 activation of soluble guanylyl cyclase: structural implication for the YC-1 binding site? Biochemistry. 43 2004; :3039–3048. DOI: 10.1021/bi0360051 [PubMed: 15023055]

60. Hatley ME, Benton BK, Xu J, Manfredi JP, Gilman AG, Sunahara RK. Isolation and characterization of constitutively active mutants of mammalian adenylyl cyclase. J Biol Chem. 275 2000; :38626–38632. DOI: 10.1074/jbc.M007148200 [PubMed: 10982815]

61. Yuen PST, Doolittleo LK, Garbers DL. Dominant negative mutants of nitric oxide-sensitive guanylyl cyclase. J Biol Chem. 269 1994; :791–793. [PubMed: 7904602]

62. Tang WJ, Stanzel M, Gilman AG. Truncation and alanine-scanning mutants of type I adenylyl cyclase. Biochemistry. 34 1995; :14563–14572. DOI: 10.1021/bi00044a035 [PubMed: 7578062]

63. Winger JA, Marletta MA. Expression and characterization of the catalytic domains of soluble guanylate cyclase: interaction with the heme domain. Biochemistry. 44 2005; :4083–4090. DOI: 10.1021/bi047601d [PubMed: 15751985]

64. Avelar GM, Schumacher RI, Zaini PA, Leonard G, Richards TA, Gomes SL. A Rhodopsin-Guanylyl cyclase gene fusion functions in visual perception in a fungus. Curr Biol. 24 2014; :1234–1240. DOI: 10.1016/j.cub.2014.04.009 [PubMed: 24835457]

65. Trieu MM, Devine EL, Lamarche LB, Ammerman AE, Greco JA, Birge RR, Theobald DL, Oprian DD. Expression, purification, and spectral tuning of RhoGC, a retinylidene/guanylyl cyclase fusion protein and optogenetics tool from the aquatic fungus Blastocladiella emersonii. J Biol Chem. 292 2017; :10379–10389. DOI: 10.1074/jbc.M117.789636 [PubMed: 28473465]

66. Chang FJ, Lemme S, Sun Q, Sunahara RK, Beuve A. Nitric oxide-dependent allosteric inhibitory role of a second nucleotide binding site in soluble guanylyl cyclase. J Biol Chem. 280 2005; :11513–11519. DOI: 10.1074/jbc.M412203200 [PubMed: 15649897]

67. Sürmeli NB, Müskens FM, Marletta MA. The influence of nitric oxide on soluble guanylate cyclase regulation by nucleotides: role of the pseudosymmetric site. J Biol Chem. 290 2015; :15570–15580. DOI: 10.1074/jbc.M115.641431 [PubMed: 25907555]

68. Wallace S, Guo DC, Regalado E, Mellor-Crummey L, Bamshad M, Nickerson DA, Dauser R, Hanchard N, Marom R, Martin E, Berka V, Sharina I, Ganesan V, Saunders D, Morris SA, Milewicz DM. Disrupted nitric oxide signaling due to GUCY1A3 mutations increases risk for moyamoya disease, achalasia and hypertension. Clin Genet. 90 2016; :351–360. DOI: 10.1111/cge.12739 [PubMed: 26777256]

69. Tesmer JJ, Sunahara RK, Johnson RA, Gosselin G, Gilman AG, Sprang SR. Two-metal-ion catalysis in adenylyl cyclase. Science. 285 1999; :756–760. DOI: 10.1126/science.285.5428.756 [PubMed: 10427002]

70. Agulló L, Buch I, Gutiérrez-de-Terán H, Garcia-Dorado D, Villà-Freixa J. Computational exploration of the binding mode of heme-dependent stimulators into the active catalytic domain

of soluble guanylate cyclase. Proteins Struct Funct Bioinf. 84 2016; :1534–1548. DOI: 10.1002/prot.25096

71. Yazawa S, Tsuchiya H, Hori H, Makino R. Functional characterization of two nucleotide-binding sites in soluble guanylate cyclase. J Biol Chem. 281 2006; :21763–21770. DOI: 10.1074/jbc.M508983200 [PubMed: 16754683]

72. Surmeli, NB; Muskens, FM; Marletta, MA. The influence of nitric oxide on soluble guanylate cyclase regulation by nucleotides: the role of pseudosymmetric site. J Biol Chem. 2015.

73. Benhar M, Forrester MT, Stamler JS. Protein denitrosylation: enzymatic mechanisms and cellular functions. Nat Rev Mol Cell Biol. 10 2009; :721–732. DOI: 10.1038/nrm2764 [PubMed: 19738628]

74. Beuve A. Thiol-based redox modulation of soluble guanylyl cyclase, the nitric oxide receptor. Antioxidants Redox Signal. 26 2016; :137–149. DOI: 10.1089/ars.2015.6591

75. Sayed N, Baskaran P, Ma X, van den Akker F, Beuve A. Desensitization of soluble guanylyl cyclase, the NO receptor, by S-nitrosylation. Proc Natl Acad Sci U S A. 104 2007; :12312–12317. DOI: 10.1073/pnas.0703944104 [PubMed: 17636120]

76. Gould NS, Evans P, Martínez-Acedo P, Marino SM, Gladyshev VN, Carroll KS, Ischiropoulos H. Site-specific proteomic mapping identifies selectively modified regulatory cysteine residues in functionally distinct protein networks. Chem Biol. 22 2015; :965–975. DOI: 10.1016/j.chembiol.2015.06.010 [PubMed: 26165157]

77. Gould N, Doulias P, Tenopoulou M, Raju K, Ischiropoulos H. Regulation of protein function and signaling by reversible cysteine S-Nitrosylation. J Biol Chem. 288 2013; :26473–26479. DOI: 10.1074/jbc.R113.460261 [PubMed: 23861393]

78. Smith BC, Marletta MA. Mechanisms of S-nitrosothiol formation and selectivity in nitric oxide signaling. Curr Opin Chem Biol. 16 2012; :498–506. DOI: 10.1016/j.cbpa.2012.10.016 [PubMed: 23127359]

79. Fernhoff NB, Derbyshire ER, Underbakke ES, Marletta MA. Heme-assisted S-nitrosation desensitizes ferric soluble guanylate cyclase to nitric oxide. J Biol Chem. 287 2012; :43053–43062. DOI: 10.1074/jbc.M112.393892 [PubMed: 23093402]

80. Beuve A, Wu C, Cui C, Liu T, Jain MR, Huang C, Yan L, Kholodovych V, Li H. Identification of novel S-nitrosation sites in soluble guanylyl cyclase, the nitric oxide receptor. J Proteomics. 138 2016; :40–47. DOI: 10.1016/j.jprot.2016.02.009 [PubMed: 26917471]

81. Crassous PA, Couloubaly S, Huang C, Zhou Z, Baskaran P, Kim DD, Papapetropoulos A, Fioramonti X, Duran WN, Beuve A. Soluble guanylyl cyclase is a target of angiotensin II-induced nitrosative stress in a hypertensive rat model. AJP Heart Circ Physiol. 303 2012; :H597–H604. DOI: 10.1152/ajpheart.00138.2012

82. Hervé D, Philippi A, Belbouab R, Zerah M, Chabrier S, Collardeau-Frachon S, Bergametti F, Essongue A, Berrou E, Krivosic V, Sainte-Rose C, Houdart E, Adam F, Billiemaz K, Lebret M, Roman S, Passemard S, Boulday G, Delaforge A, Guey S, Dray X, Chabriat H, Brouckaert P, Bryckaert M, Tournier-Lasserve E. Loss of α1β1 soluble guanylate cyclase, the major nitric oxide receptor, leads to moyamoya and achalasia. Am J Hum Genet. 94 2014; :385–394. DOI: 10.1016/j.ajhg.2014.01.018 [PubMed: 24581742]

83. Sharina I, Sobolevsky M, Doursout MF, Gryko D, Martin E. Cobinamides are novel coactivators of nitric oxide receptor that target soluble guanylyl cyclase catalytic domain. J Pharmacol Exp Therapeut. 340 2012; :723–732. DOI: 10.1124/jpet.111.186957

84. Mota F, Allerston CK, Hampden-Smith K, Garthwaite J, Selwood DL. Surface plasmon resonance using the catalytic domain of soluble guanylate cyclase allows the detection of enzyme activators. Bioorg Med Chem Lett. 24 2014; :1075–1079. DOI: 10.1016/j.bmcl.2014.01.015 [PubMed: 24480469]

85. Ben Aissa, M; Tipton, AF; Bertels, Z; Gandhi, R; Moye, LS; Novack, M; Bennett, BM; Wang, Y; Litosh, V; Lee, SH; Gaisina, IN; Thatcher, GR; Pradhan, AA. Soluble guanylyl cyclase is a critical regulator of migraine-associated pain. Cephalalgia. 2017.

86. Fernandes D, Sordi R, Pacheco LK, Nardi GM, Heckert BT, Villela CG, Lobo AR, Barja-Fidalgo C, Assreuy J. Late, but not early, inhibition of soluble guanylate cyclase decreases mortality in a rat sepsis model. J Pharmacol Exp Therapeut. 328 2009; :991–999. DOI: 10.1124/jpet.108.142034

87. Pyriochou A, Beis D, Koika V, Potytarchou C, Papadimitriou E, Zhou Z, Papapetropoulos A. Soluble guanylyl cyclase activation promotes angiogenesis. J Pharmacol Exp Therapeut. 319 2006; :663–671. DOI: 10.1124/jpet.106.108878

88. Fraser M, Chan SL, Chan SSL, Fiscus RR, Tsang BK. Regulation of p53 and suppression of apoptosis by the soluble guanylyl cyclase/cGMP pathway in human ovarian cancer cells. Oncogene. 25 2006; :2203–2212. DOI: 10.1038/sj.onc.1209251 [PubMed: 16288207]

89. Tseng KY, Caballero A, Dec A, Cass DK, Simak N, Sunu E, Park MJ, Blume SR, Sammut S, Park DJ, West AR. Inhibition of striatal soluble guanylyl cyclase-cGMP signaling reverses basal ganglia dysfunction and Akinesia in experimental parkinsonism. PLoS One. 6 2011; doi: 10.1371/journal.pone.0027187

90. Gille A, Lushington GH, Mou T, Doughty MB, Johnson RA, Seifert R. Differential inhibition of adenylyl cyclase isoforms and soluble guanylyl cyclase by purine and pyrimidine nucleotides. J Biol Chem. 279 2004; :19955–19969. DOI: 10.1074/jbc.M312560200 [PubMed: 14981084]

91. Mou T, Gille A, Suryanarayana S, Richter M, Seifert R, Sprang SR. Broad specificity of mammalian adenylyl cyclase for interaction with 2′,3′-substituted purine- and pyrimidine nucleotide inhibitors. Mol Pharmacol. 70 2006; :878–886. DOI: 10.1124/mol.106.026427 [PubMed: 16766715]

92. Suryanarayana S, Go M, Hu M, Gille A, Mou T, Sprang SR, Richter M, Seifert R. Differential inhibition of various adenylyl cyclase isoforms and soluble guanylyl cyclase by 2′,3′-O-(2,4,6-trinitrophenyl)-substituted nucleoside 5′-tri-phosphates. J Pharmacol Exp Therapeut. 330 2009; :687–695. DOI: 10.1124/jpet.109.155432.2002

93. Dove S, Danker KY, Stasch JP, Kaever V, Seifert R. Structure/activity relationships of (M)ANT- and TNP-nucleotides for inhibition of rat soluble guanylyl cyclase a1b1. Mol Pharmacol. 85 2014; :598–607. DOI: 10.1124/mol.113.091017 [PubMed: 24470063]

94. Mou TC, Gille A, Fancy DA, Seifert R, Sprang SR. Structural basis for the inhibition of mammalian membrane adenylyl cyclase by 2 "(3")-O-(N-Methylanthraniloyl)-guanosine 5′-triphosphate. J Biol Chem. 280 2005; :7253–7261. DOI: 10.1074/jbc.M409076200 [PubMed: 15591060]

95. Mota F, Gane P, Hampden-Smith K, Allerston CK, Garthwaite J, Selwood DL. A new small molecule inhibitor of soluble guanylate cyclase. Bioorg Med Chem. 23 2015; :5303–5310. DOI: 10.1016/j.bmc.2015.07.074 [PubMed: 26264842]

96. Vijayaraghavan J, Kramp K, Harris ME, van den Akker F. Inhibition of soluble guanylyl cyclase by small molecules targeting the catalytic domain. FEBS Lett. 590 2016; :3669–3680. DOI: 10.1002/1873-3468.12427 [PubMed: 27654641]

97. Haase T, Haase N, Kraehling JR, Behrends S. Fluorescent fusion proteins of soluble guanylyl cyclase indicate proximity of the heme nitric oxide domain and catalytic domain. PLoS One. 5 2010; :1–10. DOI: 10.1371/journal.pone.0011617

98. Pan J, Yuan H, Zhang X, Zhang H, Xu Q, Zhou Y, Tan L, Nagawa S, Huang ZX, Tan X. Probing the molecular mechanism of human soluble guanylate cyclase activation by no in vitro and in vivo. Sci Rep. 7 2017; doi: 10.1038/srep43112

99. Busker M, Neidhardt I, Behrends S. Nitric oxide activation of guanylate cyclase pushes the α1 signaling helix and the β1 heme-binding domain closer to the substrate-binding site. J Biol Chem. 289 2014; :476–484. DOI: 10.1074/jbc.M113.504472 [PubMed: 24220034]

100. Nienhaus GU. Exploring protein structure and dynamics under denaturing conditions by single-molecule FRET analysis. Macromol Biosci. 6 2006; :907–922. DOI: 10.1002/mabi.200600158 [PubMed: 17099864]

101. Underbakke ES, Iavarone AT, Chalmers MJ, Pascal BD, Novick S, Griffin PR, Marletta MA. Nitric oxide-induced conformational changes in soluble guanylate cyclase. Struct Des. 22 2014; :1–10. DOI: 10.1016/j.str.2014.01.008

102. Balashova N, Chang F, Lamothe M, Sun Q, Beuve A. Characterization of a novel type of endogenous activator of soluble guanylyl cyclase. J Biol Chem. 280 2005; :2186–2196. DOI: 10.1074/jbc.M411545200 [PubMed: 15509556]

103. Heckler EJ, Crassous P, Baskaran P, Beuve A. Protein disulfide-isomerase interacts with soluble guanylyl cyclase via a redox-based mechanism and modulates its activity. Biochem J. 452 2013; :161–169. DOI: 10.1042/BJ20130298 [PubMed: 23477350]

104. Heckler EJ, Kholodovych V, Jain M, Liu T, Li H. Mapping soluble guanylyl cyclase and protein disulfide isomerase regions of interaction. PLoS One. 10 2015; doi: 10.1371/journal.pone.0143523

105. Gerzer R, Hofmann F, Schultz G. Purification of a soluble, sodium-nitroprusside-stimulated guanylate cyclase from bovine lung. Eur J Biochem. 116 1981; :479–486. DOI: 10.1111/j.1432-1033.1981.tb05361.x [PubMed: 6114859]

106. Humbert P, Niroomand F, Fischer G, Mayer B, Koesling D, Hinsch K, Gausepohl H, Frank R, Schultz G, Bohme E. Purification of soluble guanylyl cyclase from bovine lung by a new immunoaffinity chromatographic method. Eur J Biochem. 190 1990; :273–278. [PubMed: 1973095]

107. Wedel B, Harteneck C, Foerster J, Friebe A, Schultz G, Koesling D. Functional domains of soluble guanylyl cyclase. J Biol Chem. 270 1995; :24871–24875. [PubMed: 7559610]

108. Gupta G, Kim J, Yang L, Sturley SL, Danziger RS. Expression and purification of soluble, active heterodimeric guanylyl cyclase from baculovirus. Protein Expr Purif. 10 1997; :325–330. DOI: 10.1006/prep.1997.0746 [PubMed: 9268679]

109. Hoenicka M, Becker E-M, Apeler H, Sirichoke T, Schröder H, Gerzer R, Stasch J-P. Purified soluble guanylyl cyclase expressed in a baculovirus/Sf9 system: stimulation by YC-1, nitric oxide, and carbon monoxide. J Mol Med. 77 1999; :14–23. DOI: 10.1007/s001090050292 [PubMed: 9930922]

110. Wagner C, Russwurm M, Jager R, Friebe A, Koesling D. Dimerization of nitric oxide-sensitive guanylyl cyclase requires the alpha-1 N terminus. J Biol Chem. 280 2005; :17687–17693. DOI: 10.1074/jbc.M412099200 [PubMed: 15749699]

111. Winger JA, Derbyshire ER, Marletta MA. Dissociation of nitric oxide from soluble guanylate cyclase and heme-nitric oxide/oxygen binding domain constructs. J Biol Chem. 282 2006; :897–907. DOI: 10.1074/jbc.M606327200 [PubMed: 17098738]

112. Derbyshire ER, Fernhoff NB, Deng S, Marletta MA. Nucleotide regulation of soluble guanylate cyclase substrate specificity. Biochemistry. 48 2009; :7519–7524. DOI: 10.1021/bi900696x [PubMed: 19527054]

113. Robert X, Gouet P. Deciphering key features in protein structures with the new ENDscript server. Nucleic Acids Res. 42 2014; :320–324. DOI: 10.1093/nar/gku316

114. McWilliam H, Li W, Uludag M, Squizzato S, Park YM, Buso N, Cowley AP, Lopez R. Analysis tool web services from the EMBL-EBI. Nucleic Acids Res. 41 2013; :597–600. DOI: 10.1093/nar/gkt376
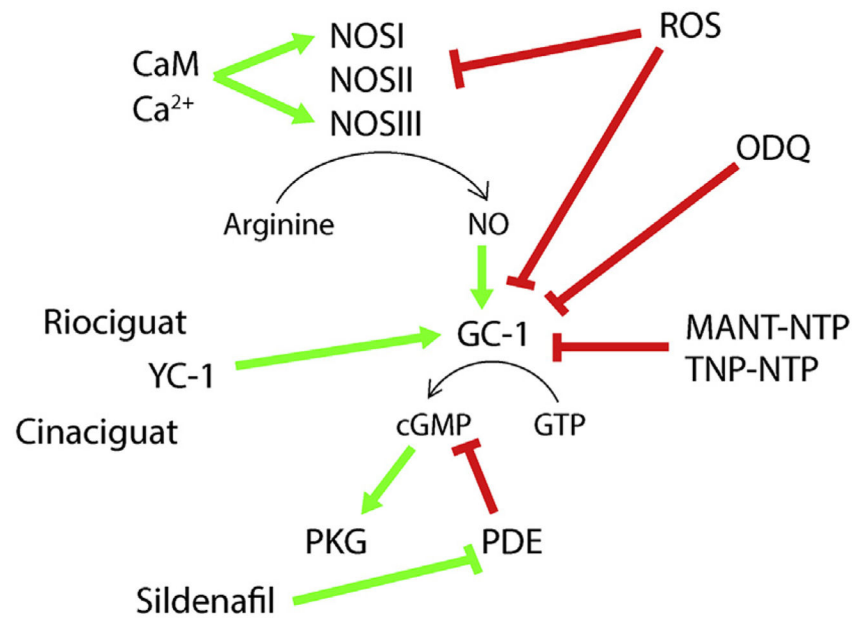
Fig. 1. Overview of the NO/GC-1/cGMP pathway

The NO/GC-1/cGMP pathway mediates vasodilation and vasoconstriction and is regulated by a variety of inhibitors and activators. Green arrows indicate pathway activation/ stimulation and red arrows indicate pathway inhibition. Abbreviations-CaM: calmodulin. NOSI/II/III: nitric oxide synthase-isoforms 1, 2, and 3. GC-1: soluble guanylyl cyclase. GTP: guanosine 5′-triphosphate. cGMP: cyclic guanosine 3′,5′-monophosphate. PKG: protein kinase G. PDE: phosphodiesterase. ROS: reactive oxygen species. ODQ: 1H-(1,2,4)oxadiazolo(4,3-*a*)quinoxaline-1-one. MANT-NTP: 2′,3′-O-(N-methylanthraniloyl) nucleotide 5′-triphosphate. TNP-NTP: 2′,3′-O-(2,4,6-trinitrophenyl) nucleotide 5′-triphosphate.
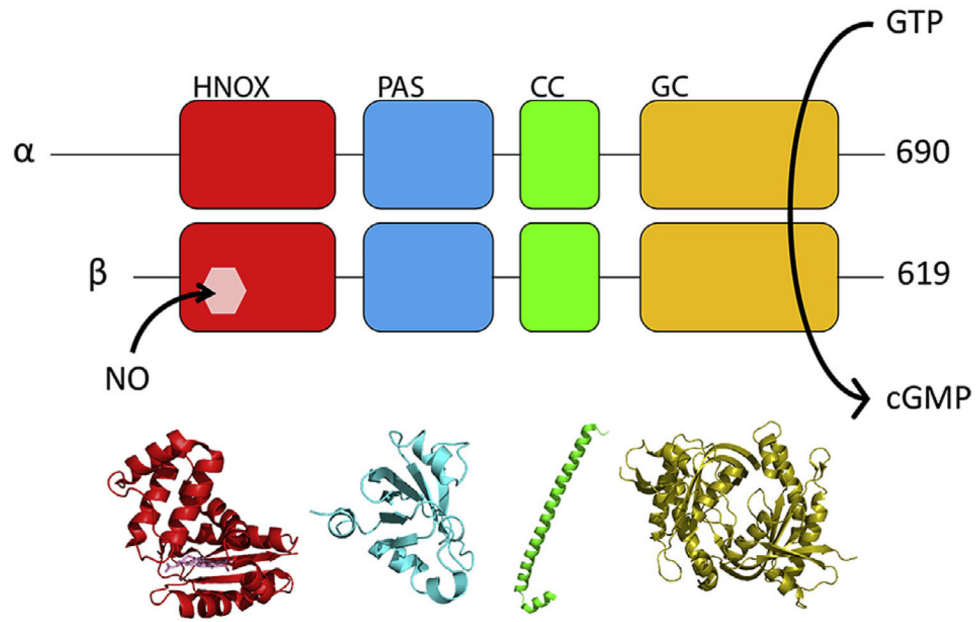
Fig. 2. GC-1 is a multi-domain enzyme

General domain architecture of GC-1 (top) and crystal structures of homologous or wild-type GC-1 domains (below). HNOX: Heme Nitric oxide-OXygen binding (PDB code 2O09, red, *Nostoc PCC 7120* HNOX). PAS: Per-Arnt-Sim (PDB code 4GJ4, cyan, *Manduca sexta* GC-1). CC: Coiled-Coil (PDB code 3HLS, green, *Rattus norvegicus* βGC-1). GC: Guanylyl Cyclase (PDB code 4NI2, gold, *Homo sapiens* αβGC-1). Numbering for the α and β chains is from *Homo sapiens* GC-1.
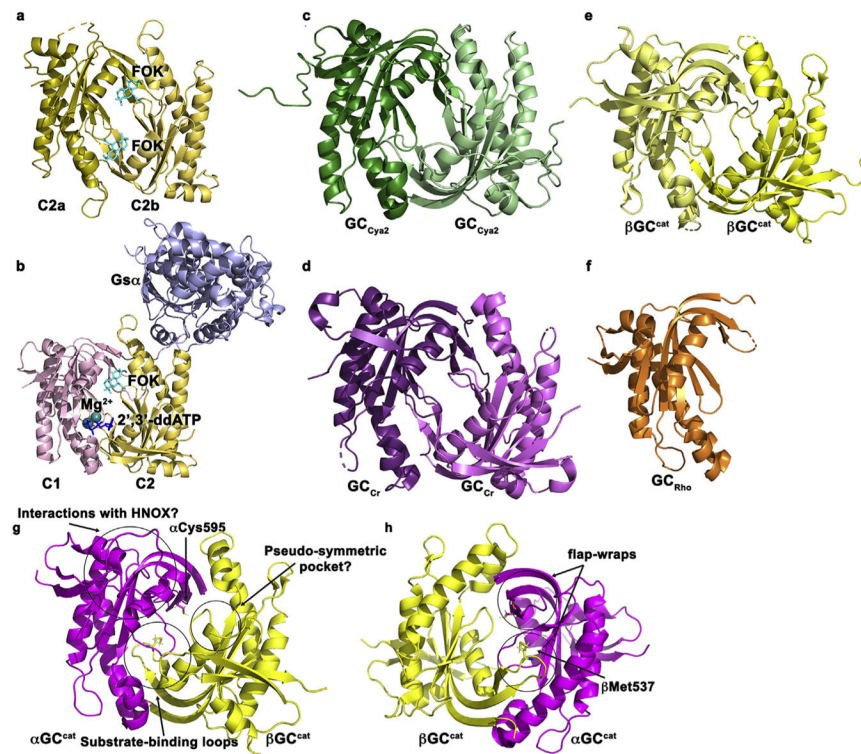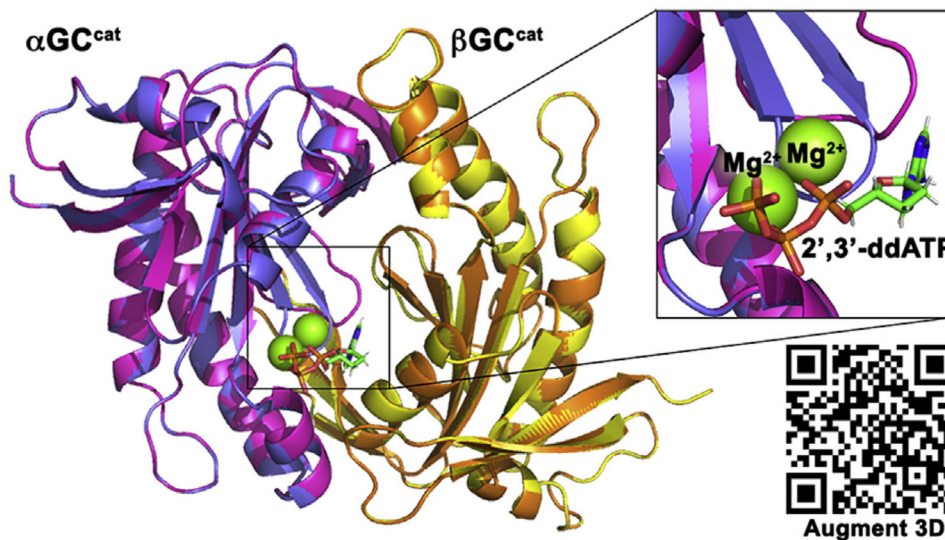
Fig. 3. Structural overview of adenylyl and guanylyl cyclases

(*a*) C2/C2 homodimer (C2a, dark/C2b, light yellow) with two forskolin molecules (FOK, cyan) at the dimer interface (PDB code 1AB8). (*b*) C1/C2 heterodimer (light red/light yellow, respectively) with bound activators $G_{s\alpha}$ (light blue) and forskolin (FOK, cyan); substrate 2′,3′-dideoxyadenosine 5′-triphosphate (2′,3′-ddATP, dark blue) and two Mg^{2+} ions (green, PDB code 1CJU). (*c*) *Synechocystis PCC 6803* Cya2 GC (GC_{Cya2}) homodimer (green, PDB code 2W01). (*d*) *Chlamydomonas reinhardtii* CYG12 GC (GC_{Cr}) homodimer (purple, PDB code 3ET6). (*e*) Human ββGCcat homodimer (dark/ light yellow, PDB code 2WZ1). (*f*) *Blastocladiella emersonii* RhoGC cyclase (GC_{Rho}) monomer (PDB code 6AO9). (*g, h*) Wild-type *Homo sapiens* αβGCcat heterodimer (αGC^{cat} magenta, βGC^{cat} yellow) and putative regions for domain activation (PDB code 4NI2) viewed on the ventral (g) and dorsal (h) side.

Fig. 4. Alignment of amino acid sequences of cyclase domains

The multi sequence alignment of guanylyl cyclase domains with available x-ray structures was performed with CLUSTAL Omega and displayed using ESpript [113,114]. The sequences used are *Homo sapiens* wild-type GC-1 αGC^{cat} and βGC^{cat} (4NI2-A and 4NI2-B, respectively), *C. reinhardtii* CYG12 GC$_{Cr}$ cyclase (3ET6), *Blastocladiella emersonii* GC$_{Rho}$ cyclase (6AO9), and *Synechotistis PCC6803* GC$_{Cya2}$ cyclase (2W01). The secondary structure elements (α helices: α1-α5, β strands: β1-β10, TT: β-turns) represented above the sequence belong to βGC^{cat}. Numbering is indicated for all sequences. Residues important for catalysis are highlighted 1–8 above the sequence alignment as in Table 1. Invariant residues are highlighted in red boxes while similar residues across all sequences are highlighted in yellow boxes. The consensus sequence (identity > 70%) is shown below the alignment. Upper case represents identity; lower case represents consensus level > 0.5; ! is anyone of IV residues, # is anyone of NDQEBZ (from BloSUM32 table), dots are residues that are not conserved. Stars above the sequence represents residues with alternate positions.

Fig. 5. Model of activated αβGC^{cat}.

Theoretical model of activated αβGC^{cat} bound to Mg^{2+} and 2,3′-ddATP. The model was obtained by superimposition of inactive αβGC^{cat} (PDB code 4NI2) on "active" adenylyl cyclase structure (PDB code 1CJU). Superposition of the inactive and active GC^{cat} subunits independently shows that the 26° rigid body rotation of the αGC^{cat} subunit around βGC^{cat} allows structural elements of both subunits to close the active site. In addition, the substrate binding loop become more structured in the active model. Inset depicts structural rearrangement at the substrate binding pocket containing two Mg^{2+} ions (green) and 2′,3′-dideoxyadenosine 5′-tri-phosphate (2,3,-ddATP). αGC^{cat} (magenta-inactive, violet-active) and βGC^{cat} (yellow-inactive, orange-active).

Table 1

Key catalytic residues in adenylyl cyclase and guanylyl cyclases.

	Metal (1)	Base (2)	Metal (3)	Phosphate (4)	Base (5)	Ribose (6)	Phosphate (7)	Phosphate (8)
AC-V C1	Asp396	(Lys436)	Asp440	Arg484	(Asp505)	–	–	–
AC-II C2	–	Lys938			Asp1018	Asn1025	Arg1029	Lys1065
αGC	Asp486	(Glu526)	Asp530	Arg574	(Cys595)	–	–	–
βGC	–	Glu473	(Asp477)		Cys541	Asn548	Arg552	Lys593
GC$_{Cr}$	Asp482	Glu520	Asp525	Arg571	Cys592	Asn599	Arg603	Lys540
GC$_{Rho}$	Asp457	Glu497	Asp501	Arg545	Cys566	Asn573	Arg577	Lys612
GC$_{cya2}$	Asp448	Glu488	Asp492	Arg450*	Gly562	Asn569	Arg573	Lys608

AC-V C1: C1 domain of *Canis lupus familiaris* adenylyl cyclase V; AC-II C2: C2 domain of *Rattus norvegicus* adenylyl cyclase II; αGC and βGC: catalytic subunits of *Homo sapiens* GC-1; GC$_{Cr}$: *C. reinhardtii* CYG12 catalytic domain; GC$_{Rho}$: *Blastocladiella emersonii* RhoGC catalytic domain; **GC$_{cya2}$**: *Synechocystis PCC 6803* Cya2 cyclase; Residues in parenthesis do not participate in the active site but are part of the pseudo-symmetric site in adenylyl cyclase, and have been shown to be important for activity in GC-1 [59]. Numbers (1)–(8) refer to amino acids highlighted in Fig. 4.

*
Arg450 in GCCya2 is structurally equivalent to Arg574 in αGC.

Table 2

Basal guanylyl cyclase activities

Comparison of reported specific activities (nmol cGMP/min/mg protein) and calculated specific activities adjusted for amounts of heterodimers (100% for GC-1) and normalized to pmol of protein (fmol cGMP/min/pmol heterodimer).

	Reported specific activity (nmol cGMP/min/mg)		Adjusted specific activity (fmol cGMP/min/pmol heterodimer)		Ref.
	Mg^{2+}	Mn^{2+}	Mg^{2+}	Mn^{2+}	
Full-length GC-1	114	610	16,876	90,301	[105]
	12.1	96	1791	14,211	[106]
	50@	400@	N/D	N/D	[107]* (?)
	22.6	N/D	3391	N/D	[108]
	46.4–153	1259	6869–22,649	186,376	[109]
	0.397@	N/D	N/D	N/D	[110]
	0.046	N/D	6.86	N/D	[111]
	152	N/D	22,501	N/D	[112]
	28	662	4145	97,955	[57]
	4300	N/D	636,551	N/D	[42]
	0.10@	N/D	N/D	N/D	[30]* (30 °C)
	2	15	296	2220	[83]
	67.7	138.3	10,075.5	20,578.5	[43]* (15 °C)
αβGC^cat	N/D	60@	N/D	N/D	[107]* (?)
	0.56	11–72	27.6#	547–3,582#	[63]
	N/D	48	N/D	2,388#	[112]
	N/D	25–300	N/D	1244–14,926#	[42]
	62	N/D	3,085#	N/D	[58]* (25 °C)
	1	N/D	49.5#	N/D	[96]
	35.4	N/D	2.2	N/D	[43]* (15 °C)
	25$	19,394$	1.4$	1,091$	[43]* (15 °C)

@ activity measured in cell lysate.

\# calculated activity assuming 100% heterodimeric $\alpha\beta GC^{cat}$.

\$ activity measured using α661-βGC^{cat} with 82.5% heterodimers as measured (30 residues truncated from αGC^{cat} C-terminus).

N/D not determined. All assays performed at 37 °C except where noted (*).